ACS OMEGA

Open Access

http://pubs.acs.org/journal/acsodf

Article

High-Efficiency and Low-Energy-Loss Organic Solar Cells Enabled by Tuning the End Group Modification of the Terthiophene-Based Acceptor Molecules to Enhance Photovoltaic Properties

Faseh Ur Rehman, Shanza Hameed, Rasheed Ahmad Khera,* Mohamed Shaban,* Manel Essid, Zouhaier Aloui, Sameerah I. Al-Saeedi, Mahmoud A. A. Ibrahim, and Muhammad Waqas*

Cite This: *ACS Omega* 2023, 8, 42492−42510

Read Online

ACCESS | Metrics & More | Article Recommendations | Supporting Information

ABSTRACT: In the current study, six nonfullerene small acceptor molecules were designed by end-group modification of terminal acceptors. Density functional theory calculations of all designed molecules were performed, and optoelectronic properties were computed by employing different functionals. Every constructed molecule has a significant bathochromic shift in the maximum absorption value (λ_{max}) except **AM6**. **AM1**−**AM4** molecules represented a narrow band gap (E_g) and low excitation energy values. The **AM1**−**AM4** and **AM6** molecules have higher electron mobility. Comparing **AM2** to the reference molecule reveals that **AM2** has higher hole mobilities. Compared to the reference molecule, all compounds have excellent light harvesting efficiency values compared to **AM1** and **AM2**. The natural transition orbital investigation showed that **AM5** and **AM6** had significant electronic transitions. The open-circuit voltage (V_{oc}) values of the computed molecules were calculated by combining the designed acceptor molecules with PTB7-Th. In light of the findings, it is concluded that the designed molecules can be further developed for organic solar cells (OSCs) with superior photovoltaic abilities.

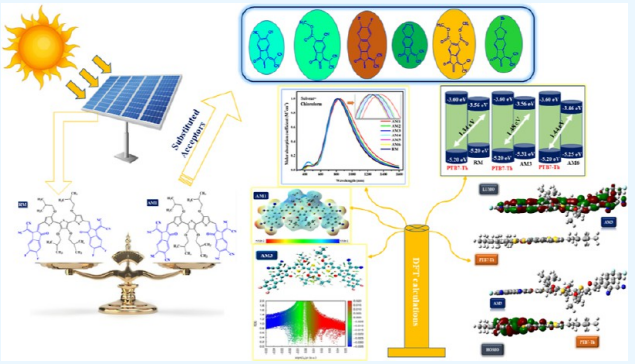

1. INTRODUCTION

Solar energy is the most innovative source of green energy with feasible properties, and photovoltaic cells play a crucial role in converting sunlight into electricity.[1] Organic solar cells have gained significant attention in recent years due to their advantages of being lightweight, low-cost, flexible, and compatible with large-area printing fabrication. Small-molecule nonfullerene organic solar cells have emerged as a promising alternative to fullerene-based organic solar cells due to their higher efficiency and better stability.[2−4] The performance of small-molecule OSCs has been rapidly increasing due to recent advances in designing and synthesizing efficient nonfullerene acceptors and optimizing device structure. Recently, up to 20% conversion efficiency has been achieved due to computational and experimental contributions.[5,6]

Recently, emerging fused ring-based highly efficient acceptors, such as ITIC and Y6, typically possess A−D−A type molecular topology with ladder-type prominent fused multidonors with electrons withdrawing acceptors on both ends as terminal acceptors (A). The large fused central core improved conjugation to lower reorganization energy for effective charge transmission and enhanced the molecules' photovoltaic capabilities. However, FREAs have very complex synthetic routes.[7] Zhenghui Yao and their co-workers developed nonfused ring acceptors to achieve low-cost and efficient organic solar cells by replacing covalent bonds with noncovalent bonds. They introduced the use of intramolecular noncovalent bonds such as (O···H, O···S, and H···F, etc.) to develop efficient small molecule acceptors (SMAs). These noncovalent bonds maintain the molecules' planarity and conformation, resulting in a highly planar structure.[8] The synthesized AOT3 acceptor molecule represented a PCE value of 6.59% based on PCE10:AOT3 type organic solar cells.

The **AOT3** molecule elaborated HOMO and LUMO values of −5.37 and −3.95 eV, respectively, along with narrow band gap values of 1.42 eV. Moreover, the **AOT3**-based device has photovoltaic properties such as V_{oc} 0.62 V, J_{sc} values of 17.63 mA cm^{-2}, and FF values up to 0.59.[9] We selected this molecule as a reference while considering all these efficient properties of the AOT3 molecule. The central donor part of this molecule consists of a (3,3′,4′,3″-Tetraisobutoxy-5-methyl-[2,2′; 5′,2″] terthiophene)-based central donor part, and the terminal

Received: July 18, 2023
Accepted: October 9, 2023
Published: November 1, 2023

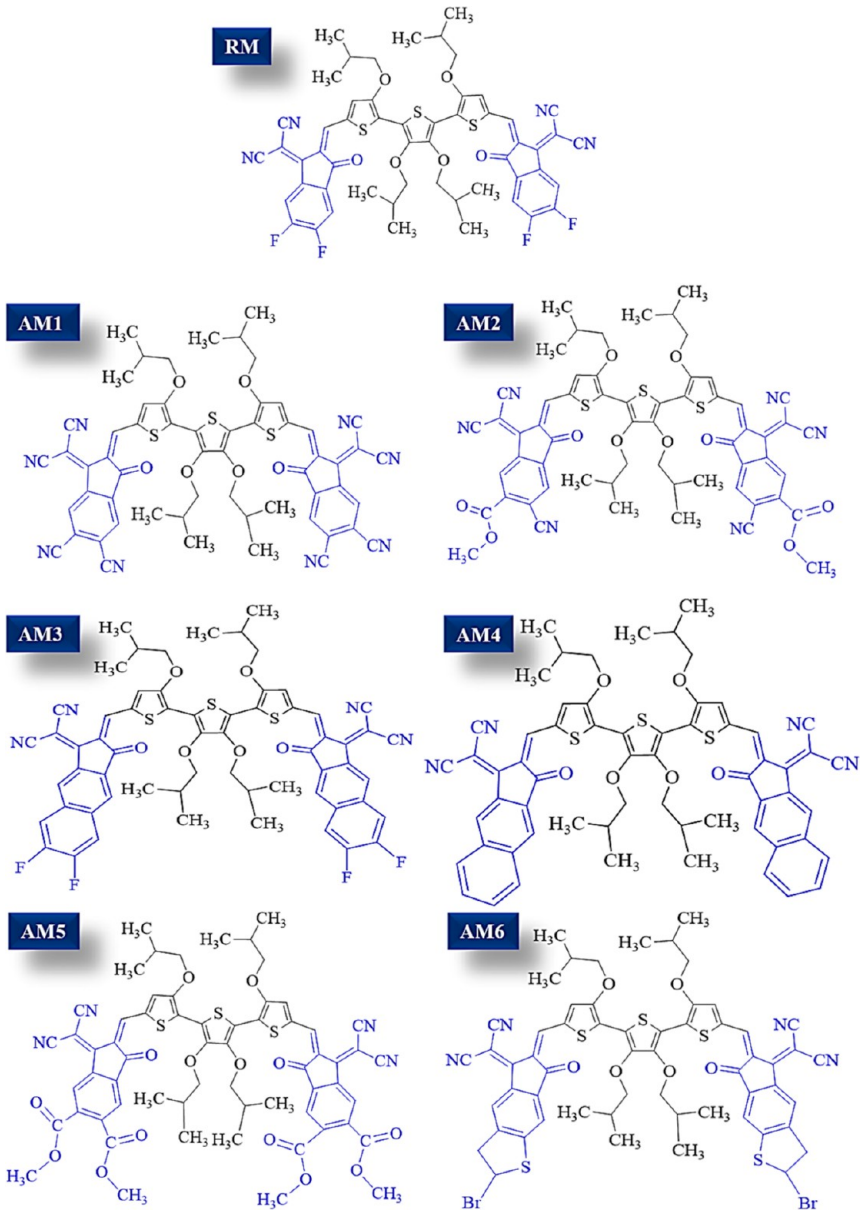

Figure 1. ChemDraw structures of **RM** and **AM1−AM6** molecules.

acceptor contains a 2-(5,6-difluoro-2-methylene-3-oxo-indan-1-ylidene)-malononitrile type group. The structural composition of donor and acceptor materials plays a crucial role in reducing recombination losses and molecular charge transfer.[10]

There has been growing interest in studying end-cap modification of small molecule acceptors for OSCs in recent years. By tailoring the end-cap groups, researchers aim to manipulate the absorption spectra, energy levels, charge transport abilities, and, ultimately, the power conversion efficiency of organic solar cells.[11−13] Many research groups have reported that end-cap modification can significantly improve the photovoltaic properties of OSCs.[14] For example, one study reported that end-capping a nonfullerene acceptor with electron-withdrawing groups resulted in an increase in V_{oc} of 0.25 V and an increase in FF of 0.05.[15,16] Similarly, end-capping a nonfullerene acceptor with solubilizing groups increased the short-circuit current density to 10 mA/cm^2.[17]

The AOT3 molecule has excellent chromophoric absorption and V_{oc} value. But to improve the photovoltaic absorption open circuit voltage and reduce the reorganization energies, we computationally substituted this terminal acceptor group with six different electron-withdrawing acceptors as a result of six novel molecules designed. For convenient comparison between designed and reference (AOT3) molecules,[9] **the AOT3** molecule was renamed **RM**. The computationally scrutinized molecules are **AM1-AM6**, and substituted acceptors are 1-dicyanomethylene-2-methylene-3-oxo-indan-5,6-dicarbonitrile (**AM1**), 6-cyano-3-dicyanomethylene-2-methylene-1-oxo-indan-5-carboxylic acid methyl ester (**AM2**), 2-(6,7-difluoro-2-methylene-3-oxo-2,3-dihydro-cyclopenta[*b*]naphthalen-1-ylidene)-malononitrile (**AM3**), 2-(2-methylene-3-oxo-2,3-dihydro-cyclopenta[*b*]naphthalen-1-ylidene)-malononitrile (**AM4**), 1-dicyanomethylene-2-methylene-3-oxo-indan-5,6-dicarboxylic acid dimethyl ester (**AM5**), and 2-(2-bromo-6-methylene-7-oxo-2,3,6,7-tetrahydro-1-thia-*s*-indacen-5-ylidene)-malononitrile (**AM6**), as represented in Figure 1.

These scrutinized acceptors are considered to give superior outcomes for efficient OSCs.[18] All investigated compounds

https://doi.org/10.1021/acsomega.3c05176
ACS Omega 2023, 8, 42492−42510

showed potential photovoltaic and optoelectronic properties, such as reduced band gap, efficient light absorption properties, improved open circuit voltage, and excellent electronic transitions in natural transition orbitals. In the long run, all of the investigated compounds can be viable for producing efficient NFSMA-based organic solar cells.

2. COMPUTATIONAL DETAILS

The visualization and construction of the studied molecules were performed by GaussView 6.0.16 software.[19] However, Gaussian 0.9 software was used to study the computational details of these molecules.[20] Therefore, for the confirmation of the functionality of our analysis, four essential and common functional B3LYP,[21] CAM-B3LYP,[22] MPW1PW91,[23] and WB97XD,[24] at a 6-31G basis set of time-dependent application of modern density functional theory (TD-DFT) were run for the **RM** molecule. The results of the highest absorption wavelength (λ_{max}) in the $CHCl_3$ solvent were compared with the cited experimental λ_{max} in the reference paper,[9] as shown in Figure 2. To simulate the environment of the chloroform

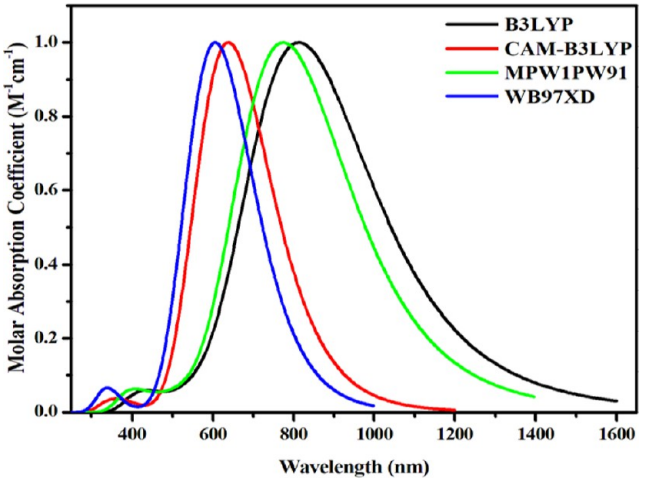

Figure 2. Absorption λ_{max} of **RM** with different examined functionals.

solvent medium, the integral equation formalism polarizable continuum model (IEFPCM) was utilized.[25] In this manner, the functional (B3LYP) was selected for further calculation due to its closest λ_{max} (814 nm) value to the cited λ_{max} (810 nm) value. The results of all the above-utilized functionals are shown graphically by using Origin 6.0. software.[26]

Further computations were performed on the proposed molecules using the B3LYP functional at a restricted spin state. The restricted spin was used to prevent any potential spin contamination. All our proposed molecules are investigated for the band gap present between the frontier molecular orbitals and their ground-state geometries. Moreover, to analyze the molecules' conjugation and planarity, the bond length and dihedral angle are calculated at the points of the donor and acceptor substitution regions of the molecules. The excited state energy analysis includes the density of state (DOS) and transition density matrix (TDM) analysis. The density of state visualized and calculated by PyMOlyze1.1 software[27] provides us with the contribution of each orbital in the radiation absorption. While TDM was plotted by Multiwfn 3.7 software,[28] plots provide information about charge delocalization and the localization of proposed molecules. The Marcus theory has been used to calculate the intermolecular and intramolecular charge movements, and the reorganization energy has been examined. Instead, in this study, we concentrated on intramolecular charge transfer (ICT).[29] The term "reorganization energy" (RE) describes the interaction of two separate but connected reorganization energies. External RE is influenced by powerful polarity fluctuations and environmental oscillations that occur throughout the charge transfer; internal RE mainly relies on changes in the molecular structure. We are limited to using internal RE for this analysis because we cannot employ external RE to validate our calculations.[30] The RE values for λ_+ and λ_- were calculated using eqs 1 and 2

$$\lambda_+ = [E_+^0 - E_0] + [E_+^0 - E_+] \quad (1)$$

$$\lambda_- = [E_-^0 - E_0] + [E_0^- - E_-] \quad (2)$$

In the above equations, E_+^0 and E_-^0 signify the neutral energies of optimized cation and anion molecules. The E_0^+ and E_0^- are the cation and anion energies; these energies are obtained from the neutral molecule's optimization at the ground state. The optimized geometry of the molecules examines the E^+ and E^- energies.[31]

Lastly, photovoltaic properties such as fill factor (FF) and open circuit voltage are directly linked to the PCE and were also examined for the proposed molecules. This resulted in better photovoltaic analysis in the active layer of the concerned organic-photovoltaic cell.[32]

3. RESULTS AND DISCUSSION

3.1. Ground-State Geometrical Analysis. The optimization of all molecules was done to examine the frontier molecular orbitals and the geometry of the molecules. Moreover, the ground-state optimization of the molecules is necessary for proper analysis of the optoelectronic attributes of the molecules.[33] It provides information about the molecular structure and electronic properties that are essential for understanding photovoltaic performance. The arrangement of atoms in a molecule significantly influences its electronic and optical properties. For instance, the distance between donor and acceptor moieties impacts their charge transfer characteristics. Accurate optimization helps determine the most stable and relevant molecular configuration for subsequent calculations. Ground-state optimization yields the electronic structure of molecules, including the distribution of electrons and the energy levels of molecular orbitals. This information is crucial for understanding charge carrier transport recombination and determining the open-circuit voltage (V_{OC}).

Furthermore, the ground-state structure of a molecule determines its electronic properties, such as its HOMO (highest occupied molecular orbital) and LUMO (lowest unoccupied molecular orbital) energy levels. These energy levels are critical in determining the molecule's ability to absorb light and transport charge. For these reasons, it is crucial to optimize the ground-state structure of molecules before analyzing their optoelectronic properties. Therefore, after properly optimizing all the studied molecules, the bond length and dihedral angle values were measured at the substitution points of the donor and acceptor parts of the molecule. The optimized geometries of RM and all the designed AM1−AM6 molecules are shown in Figure 3. Both the bond length and dihedral angle values of all of the molecules are shown in Table 1. The values of these parameters are calculated between the central donor (core)

https://doi.org/10.1021/acsomega.3c05176
ACS Omega 2023, 8, 42492−42510

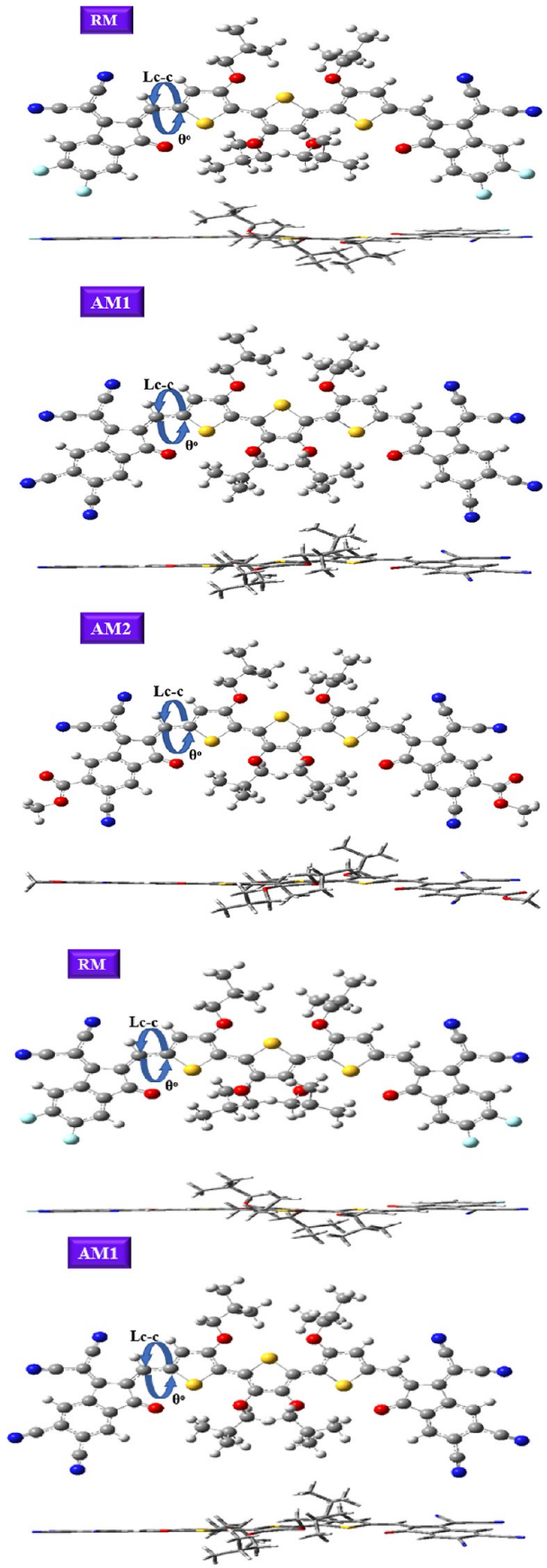

Figure 3. Optimized structures of **RM** and **AM1**−**AM6** molecules.

Table 1. Computed Geometrical Values of the RM and AM1−AM6 Molecules

molecules	bond length (L_{c-c}) (Å)	dihedral angle ($\theta°$)
RM	1.44	1.95
AM1	1.41	1.32
AM2	1.41	1.04
AM3	1.41	1.53
AM4	1.41	1.07
AM5	1.41	0.97
AM6	1.41	1.50

and terminal acceptors of the molecule because structural modifications are done at the points in this study. These play a promising role in explaining the planarity and conjugation of the molecules. It can be seen from the tabulated data that the bond length in all the studied molecules is 1.41 Å. This value lies in the range of single bond length L_{c-c} (1.54 Å) and double bond length (1.34 Å), which is appropriate for the presence of significant conjugation in the molecule.[34] Therefore, it can be concluded that a substantial conjugation is present in **AM1**−**AM6** molecules, leading to a prominent charge present within these molecules.

The dihedral angle ($\theta°$) values are also calculated between the molecule's central donor (core) and terminal acceptors. The dihedral angle value of the **RM** molecule is 1.95°, while for the proposed molecules, the values are 1.32, 1.04, 1.53, 1.07, 0.97, and 1.50° for **AM1**, **AM2**, **AM3**, **AM4**, **AM5**, and **AM6** molecules, respectively. In comparison, the dihedral angle values of all of the designed molecules are less than those of the **RM** molecule, representing the presence of high planarity, π-conjugation, and excellent charge mobility among the acceptor and donor parts of the designed molecules. The **AM5** molecule represents the lowest dihedral angle values compared to **RM**; this represents the high planar structure of this molecule.

3.2. Detailed Planarity Analysis. Moreover, for a detailed evaluation of the planarity of all the studied molecules, the molecular planarity parameters (MPP) and span of deviation from the plane (SDP) values are calculated and tabulated in Table 2 and can be visualized in Figure 4. Smaller values of

Table 2. Computed Planarity Parameters of the RM and AM1−AM6 Molecules

molecules	MPP	SDP	MPD	MND
RM	0.206909	0.843132	0.39888	−0.44425
AM1	0.354319	1.544146	0.79926	−0.74488
AM2	0.372265	1.579746	0.78983	−0.77991
AM3	0.441648	1.857450	0.93423	−0.92322
AM4	0.383209	1.540872	0.80429	−0.73658
AM5	0.537946	3.565913	1.64215	−1.92376
AM6	0.382709	1.577933	0.79577	−0.78217

MPP and SDP show the excellent planarity of that molecule. Higher values of MPP and SDP represent a low degree of planarity. In another sense, the planarity of the molecules has an inverse relationship with the MPP and SDP values of the molecules.[35,36] The MPP value of **RM** is 0.20 Å, which implies that this molecule's donor and acceptor regions are highly planar. Among the proposed molecules, **AM1** represents the lowest MPP (0.354319 Å) and SDP (1.544146 Å) values due

https://doi.org/10.1021/acsomega.3c05176
ACS Omega 2023, 8, 42492−42510

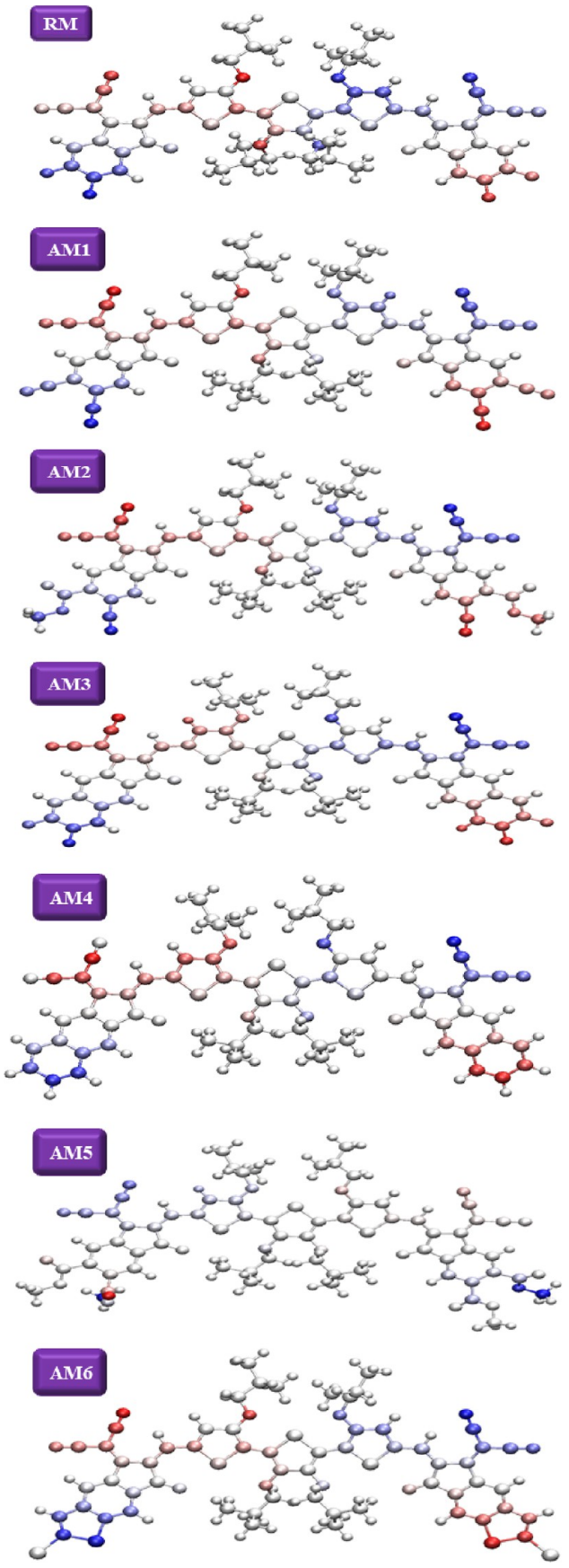

Figure 4. Planarity structures of **RM** and **AM1−AM6** molecules.

to the smaller −CN group in the terminal acceptors of these molecules.

However, **AM5** has higher SDP values (3.565913 Å) due to ester-containing acceptor groups, representing a higher structural part deviation to minimize steric hindrance between them. Figure 4 also shows the deviation of each part of the molecule from the plane. The red color shows the areas below the fitted plane, and the blue color shows the areas above the fitted plane. The silver color of the molecules shows that regions are within the fitted plane. The MPD (maximal positive deviation) and MND (maximal negative deviation) evaluations revealed the positive and negative deviation of atoms from the plane.[37] **AM5** molecules represent higher MPD (1.64215 Å) and MND values (−1.92376 Å), elaborating the highest positive and negative deviation of atoms from the plane. At the same time, **AM2** exhibits the least MPD (0.78983) among all designs designed to explore the minimum positive deviation from the plane. Eventually, all the studied molecules' MPP, SDP, MPD, and MND values are insignificant and represent almost planar structures.

3.3. Frontier Molecular Orbital Analysis. The frontier molecular orbital (FMO) analysis is crucial because it reveals how effectively the molecules enable charge transfer and electric charge dispersion. It helps to comprehend how charges are distributed and promoted within OSCs.[38] The highest occupied molecular orbital (HOMO) as well as the lowest unoccupied molecular orbital (LUMO) energies of the molecules have a prominent impact on their electrical properties, such as absorptivity, conduction process, and other electrical features.[39] While addressing OSCs and other photovoltaic procedures, it is essential to include the energy gap (E_g), which represents the energy required for electronic excitations. It has been observed that molecules with smaller band gaps typically have low open-circuit voltages but absorb more sunlight, resulting in higher current production and vice versa. Hence, the band gap must be within an optimized range for a molecule to produce efficient photovoltaic properties for all the examined factors.[40] The molecules that exhibit low E_g values are incredibly polarizable, very reactive, and possess weak reaction kinetics.[41] The computed FMOs and E_g energies of the **RM** and **AM1−AM6** molecules are examined to calculate the impact of various electron-accepting energy gaps on the photochemical properties of the molecules under study. The HOMO and LUMO values of all studied molecules are listed in Table 3 and Figure 5.

The charge density mainly resided on the molecules' central core, the donor part. The charge density is present in the excited state on the end group accepting subunits. The **RM** molecule has HOMO, LUMO, and energy gap (E_g) values of −5.33, −3.56, and 1.77 eV, respectively. AM1 has a highly

Table 3. HOMO Level, LUMO Level, and E_g Values of RM and AM1−AM6 Molecules are Given in eV

molecules	E_{HOMO} (eV)	E_{LUMO} (eV)	E_g (eV)
RM	−5.33	−3.56	1.77
AM1	−5.78	−4.08	1.70
AM2	−5.53	−3.79	1.74
AM3	−5.31	−3.56	1.75
AM4	−5.19	−3.42	1.76
AM5	−5.38	−3.60	1.78
AM6	−5.25	−3.46	1.79

https://doi.org/10.1021/acsomega.3c05176
ACS Omega 2023, 8, 42492−42510

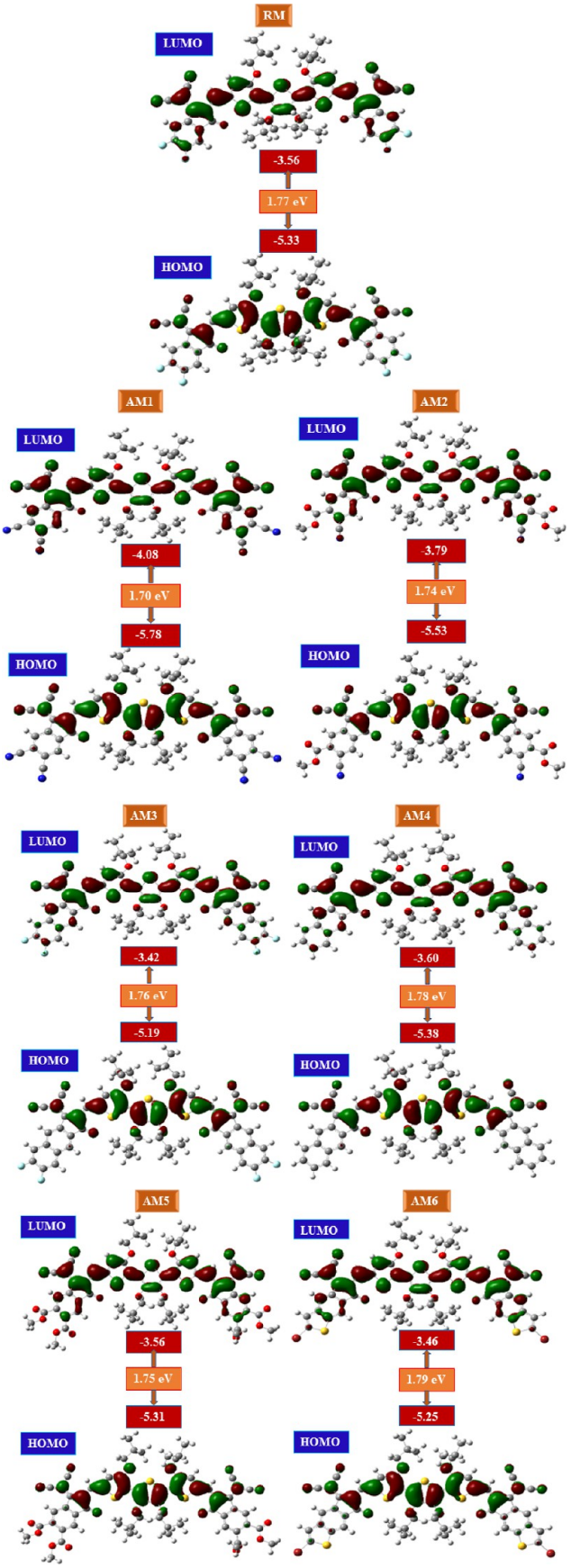

Figure 5. FMOs of **RM** and **AM1**−**AM6** molecules.

stable HOMO compared to all tested molecules, with a HOMO value of −5.78 eV. The extraordinarily stable ground state of the **AM1** molecule is due to excellent electrostatic dispersion, which resulted from four electron-withdrawing −**CN** groups present in the acceptor regions of this molecule. The **AM2** molecule also exhibits highly stable HOMO after AM1, **possibly** due to a low HOMO value of −5.53 eV. The presence of −CN and ester electron-withdrawing moieties in the end group (EG) of **AM2** is the most appropriate for this stable HOMO. The decreasing patterns of HOMO and LUMO orbitals energies are **AM1** > **AM2** > **AM5** > **RM** > **AM6** > **AM4** and **AM1** > **AM2** > **AM5** > **AM3** = **RM** > **AM6** > **AM4**. The E_g value of every designed molecule has decreased compared to that of **RM**, except for **AM5** and **AM6** molecules. The increase in E_g values of these molecules due to prominent electron-withdrawing acceptors results in better charge transfer ability in these molecules. The decreasing pattern of band gap values for all the computationally examined molecules is as follows: **AM6** > **AM5** > **RM** > **AM4** > **AM3** > **AM2** > **AM1**. **AM5** and **AM6** show maximum band gap values. The band gap of all these studied molecules was calculated as the difference between their HOMO and LUMO energy levels. FMO analysis revealed that the HOMO and LUMO of **AM5** and **AM6** have higher energy gaps, which signifies their increased band gap. **AM5** has low-lying HOMO and LUMO, while **AM6** has high-lying HOMO and LUMO energy levels. These energy levels are pretty far from each other, resulting in an increased energy gap. However, the band gap of these molecules is not too high compared to **RM**, making them usable candidates for OSC applications.

3.4. Natural Transition Orbital Analysis. Natural transition orbitals (NTOs) precisely consist of electrons (which act similarly to HOMO) and holes (which act similarly to LUMO). As in NTOs, electronic excitations also occur from HOMO to LUMO orbitals of the same molecule, such as HOMO − 1 to LUMO + 1 excitations.[42] In NTOs, the HOMO and LUMO energy gap is more significant due to the prominent separation of both energy levels; however, in typical molecular orbital excitations, the energy gap is smaller due to the mixing of electronic excitations between various HOMO and LUMO energy levels.[43] While visualizing the NTOs in Gauss view, the orbital values depict the numbers of occupied electrons rather than the orbital energies.[43] The NTOs analysis of **RM** and scrutinized molecules (**AM1**−**AM6**) was performed at the excitation possessing the highest oscillator strength value (f). The HOMO to LUMO electronic transitions are listed in Table 6 and shown in Figure 6. f is an analysis of the extent of the electronic transitions to the provided excited state. Therefore, a transition state depicting the highest f might also exhibit the highest λ_{max} values. The **AM5** and **AM6**

Table 4. Computationally Calculated IP and EA of All of the Studied Molecules

molecules	IP (eV)	EA (eV)
RM	0.22	0.10
AM1	0.24	0.12
AM2	0.23	0.10
AM3	0.22	0.10
AM4	0.22	0.09
AM5	0.22	0.10
AM6	0.22	0.09

https://doi.org/10.1021/acsomega.3c05176
ACS Omega 2023, 8, 42492−42510

Table 5. All Analyzed Molecules' LHE, Oxidation Potential, and Excited State Lifetime Values

molecules	LHE	oxidation potential (E_{ox}) eV	excited state lifetime (τ) ns
RM	0.9951	5.33	0.27
AM1	0.9933	5.78	0.33
AM2	0.9944	5.53	0.30
AM3	0.9971	5.31	0.26
AM4	0.9971	5.19	0.25
AM5	0.9958	5.38	0.27
AM6	0.9972	5.25	0.25

Table 6. Calculated λ_{max}, E_x, Oscillator Strength, and Percentage ECT Values of RM and AM1−AM6 in the Gaseous Phase

molecules	calculated λ_{max} (nm)	excitation energies E_x (eV)	oscillator strength (f)	percentage ECT (%)
RM	738	1.6793	2.0829	100
AM1	771	1.6068	1.9749	98
AM2	755	1.6413	2.0584	99
AM3	754	1.6434	2.2988	100
AM4	748	1.6562	2.2926	100
AM5	741	1.6726	2.1669	100
AM6	740	1.6742	2.3342	100

molecules represent 100% electronic transitions at the highest excited state 1. Thus, the maximum electron movement occurs from HOMO to these molecules' hole (LUMO) regions. These results eventually represent that in the charge transfer complexes, the electrons and holes are concentrated on the specific atomic regions, enabling $n-\pi^*$ transitions of these studied molecules.

3.5. Ionization Potential and Electron Affinity Analysis. Many factors, such as IP (ionization potential) and EA (electron affinity), may impact how effectively charges are transferred. EA is the energy released after adding an e− to a molecule, whereas IP is the energy required for removing an electron.[44] A molecule with high IP and EA values has highly stable HOMO, which results in the complicated removal of electrons, and electrons can be quickly released from a molecule with low IP and EA values.[41] The electron-withdrawing acceptor group stabilizing the HOMO orbital gave molecules with higher IP and EA values. However, the donor group's low IP and EA values destabilized the HOMO orbital.[45] Equations 3 and 4 were used to calculate the IP and EA values.

$$\mathbf{IP} = [E_0^+ - E_0] \quad (3)$$

$$\mathbf{EA} = [E_0 - E_0^-] \quad (4)$$

Table 4 shows the IP and EA values of **RM** and all of the designed molecules **AM1−AM6**. It can be seen that **AM1** exhibits the highest IP and EA values of all the examined molecules, which resulted in a highly stabilized HOMO (−5.78 eV) of this molecule. **AM4** and **AM6** molecules also represent lower IP (0.22) and EA (0.09) values, destabilizing the HOMO and resulting in efficient charge transfer in these molecules.

3.6. Optical Property Analysis. Generally, a molecule's absorption properties are prominent in determining the remarkableness of any organic photovoltaic (OPV) chromophore. Therefore, by utilizing the Origin 6.0 software, the UV/

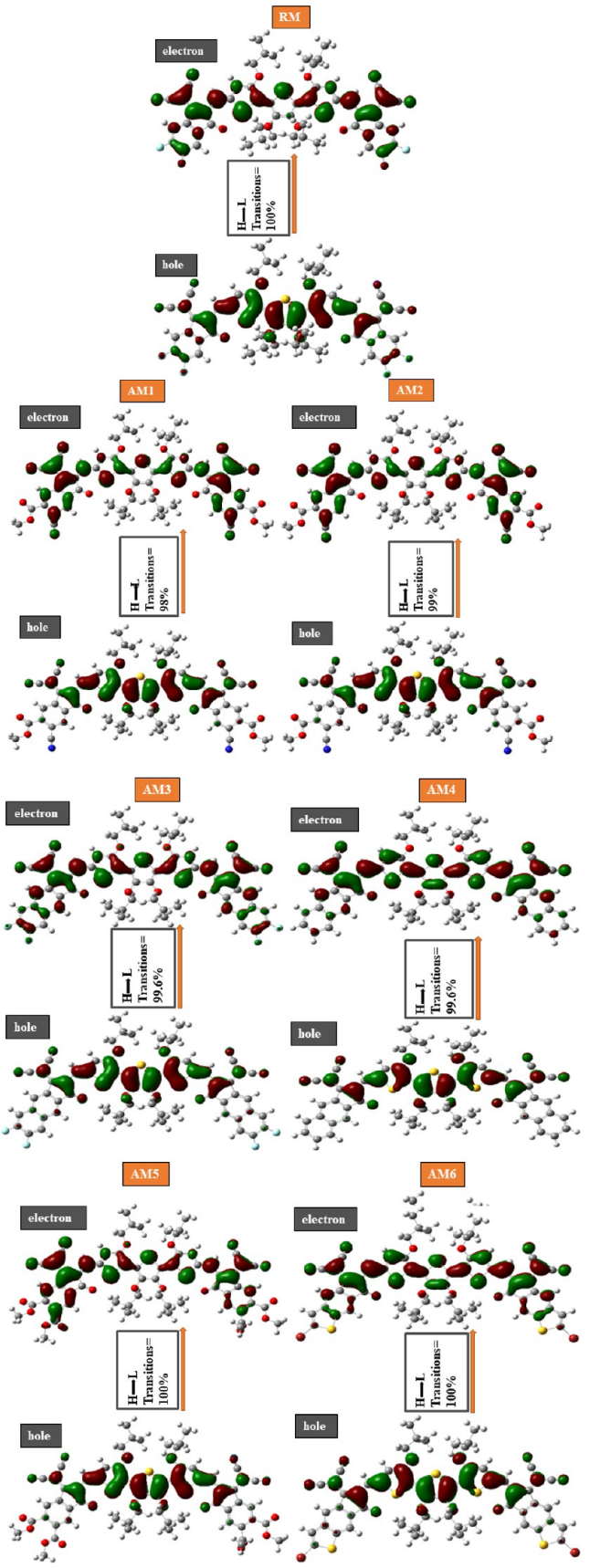

Figure 6. NTO structures and the percentage **ECT** of **RM** and **AM1−AM6**.

https://doi.org/10.1021/acsomega.3c05176
ACS Omega 2023, 8, 42492−42510

visible spectra of the examined molecules in gaseous and solvent phases (chloroform) were mapped to assess the absorption capacities of these molecules. Therefore, the maximum absorption wavelength (λ_{max}) was attained from these absorption spectra. In contrast, λ_{max} is also considered the most essential factor in determining the absorption abilities of a molecule.[29] Moreover, oscillator strength, excitation energy, ground and excited state dipole moments, and the percent transitions from HOMO to LUMO in all proposed molecules were determined in both assessed phases. The conclusions for all these investigated characteristics in both analyzed phases are compiled in Tables 6 and 7, respectively. Moreover, parts a and b of Figure 7a,b represent the absorption λ_{max} spectrum and bar graph comparison of computed λ_{max} with *R*.

Table 7. Computed λ_{max}, Excitation Energy, and Oscillator Strength Values of all the Studied Molecules in a Chloroform Solvent

molecules	exp. λ_{max} (nm)	calculated λ_{max} (nm)	excitation energies E_x (eV)	oscillator strength (f)
RM	810	814	1.5219	2.3148
AM1		859	1.4419	2.1795
AM2		839	1.4774	2.2568
AM3		827	1.4990	2.5470
AM4		820	1.5112	2.5453
AM5		818	1.5155	2.3779
AM6		810	1.5296	2.5555

Briefly said, reduced electronic band gap (E_g) or excitation energy, oscillator strength, and larger max, as well as a broad absorbance spectrum, are likely to be desirable for the excellent operation of an organic photovoltaic (OPV) cell.[46] Table 5 represents the absorption maximum of **RM** and all the studied molecules **AM1−AM6** in the gaseous phase, possessing values of 738, 771, 755, 754, 748, and 741 and 740, 755, 754, 748, 741, and 740 nm, respectively. Table 6 represents the absorption (λ_{max}) in the chloroform solvent phase. The declining trend of (λ_{max}) in the solvent phase is as **AM1** > **AM2** > **AM3** > **AM4** > **AM5** > **RM** > **AM6**, and their values are 814, 859, 839, 827, 820, 818, and 810 nm, respectively. All the designed molecules represent redshift in the λ_{max} due to the excellent stability of delocalized e− in chloroform solvent. The **AM1** and **AM2** molecules represent the highest λ_{max} values in both gaseous and solvent phases due to the presence of the −CN group and −CN ester groups in the terminal acceptors of these molecules, respectively. It can be concluded that **AM1** and **AM2** are the best chromophores of all of the examined molecules.

The excitation energy (E_x), also known as the electronic band gap, is an essential parameter in examining the efficiency of OSCs. It is the minimal energy required to transition an electron from its ground state to its excited state. In this analysis, we only determined the first electronic band gap; the maximum (99%) excitations of λ_{max} were observed from HOMO to LUMO orbital energy levels.[47] The increasing pattern of first excitation energies of all the examined molecules in the solvent phase is **AM1** < **AM2** < **AM3** < **AM4** < **AM5** < **RM** < **AM6**, and in the gaseous phase it is **AM1** < **AM2** < **AM3** < **AM4** < **AM5** < **AM6** and **RM**, respectively. It can be observed from the above patterns that **AM1** and **AM2** have the lowest excitation energies in both phases.

Oscillator strength (f) shows the potential for electron transitions after radiation absorption. It has a direct relationship with the light-harvesting efficiency (LHE) of any molecule under consideration (an essential factor for examining the short-circuit current density value), and it is a dimensionless quantity.[48] Furthermore, expanding the absorption range, decreasing E_x, or raising f could all improve ICT.[49] Tables 5 and 6 show that all of the molecules under study could perform with comparable (f) values in both phases. However, **AM1** molecules represent the lowest oscillator strength value concerning the **RM** molecule.

Each solar cell component must be able to generate an electric current after being exposed to light, which is referred to as light harvesting efficiency.[50] LHE and oscillator strength affect the absorption of the solar system; as a result, the extent of short circuit current density (J_{sc}) is produced.[51] eq 5 was utilized to calculate the LHE value of each studied compound.

$$\mathbf{LHE} = 1 - 10^{-f} \tag{5}$$

Table 5 represents the calculated LHE values of the **RM** and **AM1−AM6** molecules in the chloroform solvent. The increasing trend of LHE values is **AM1** < **AM2** < **RM** < **AM5** < **AM3** = **AM4** < **AM6**. It can be seen that **AM1** and **AM2** molecules represent fewer LHE values due to the negative impact of end group acceptors on electronic transition probability, resulting in reduced LHE values. Concisely, the LHE values of all of the examined molecules are higher than RM molecules, except **AM1** and **AM2** molecules.

3.6.1. Oxidation Potential. The oxidation potential is a necessary parameter that plays a crucial role in explaining the photovoltaic properties of organic solar cells. It is related to the HOMO energy level of the molecule, as a higher HOMO value results in a greater oxidation potential of the concerned molecule.[52] The oxidation potential values of **RM** and all designed chromophores (**AM1−AM6**) were calculated by eq 6 and illustrated in Table 5.

$$E_{ox} = -\mathbf{HOMO} \tag{6}$$

Where E_{ox} represents the oxidation potential, and -**HOMO** elaborates a negative of homo values. The decreasing pattern of examined oxidation potential values of reference (**RM**) and all modeled chromophores (**AM1−AM6**) is as follows **AM1** (5.78 eV) > **AM2** (5.53 eV) > **AM5** (5.38 eV) > **RM** (5.33 eV) > **AM3** (5.31 eV) > **AM6** (5.25 eV) > **AM4** (5.19 eV). The pattern shown above shows that **AM1** and **AM2** molecules elaborated the highest oxidation potential, consequently acting as excellent acceptor molecules. The results of the investigated optical and electronic properties of all these molecules give us fruitful information about the absorption behavior of these molecules. The higher maximum absorption wavelength points of newly designed molecules suggest that these molecules have improved capability for light absorption compared to reference molecules. The absorption graphs of all molecules validate this aspect. Similarly, low excitation energy values indicate that electrons in these molecules can be easily excited, i.e., by absorbing less energy than RM. Improved oscillator strength signifies the improved ability of these molecules to absorb more light energy.

3.6.2. Excited State Lifetime (τ) Analysis. One key factor influencing the charge transfer efficiency is the excited state lifetime (τ). A chromophore with extended τ values might exhibit more convenient charge transfer abilities.[53] The τ

https://doi.org/10.1021/acsomega.3c05176
ACS Omega 2023, 8, 42492−42510

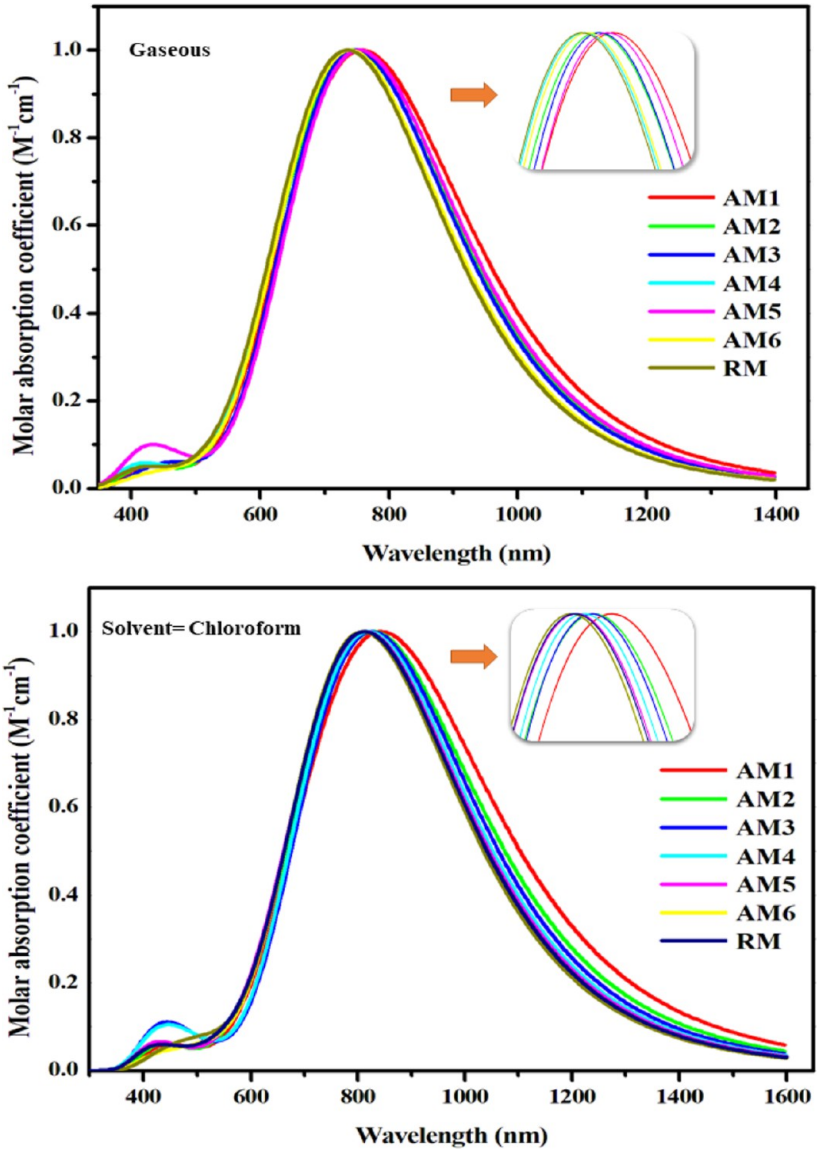

Figure 7. Absorption λ_{max} spectrum and of **RM** and **AM1−AM6** in the gaseous and solvent phase.

values of **RM** and all modeled chromophores **AM1−AM6** were calculated by eq 7, and the values are represented in Table 5.

$$\tau = 1.499/fE_{ex}^2 \quad (7)$$

Here, E elaborates on the energy of the transition at different excited states, and f depicts the oscillator strength of the excited state. The decreasing trend of τ values for all of the studied molecules is as follows: **AM1** > **AM2** > **RM** = **AM5** > **AM3** > **AM4** = **AM6**. The above trend shows that AM1 and **AM2** molecules represented larger τ values than the **RM**. As a result, these molecules exhibit easier charge transfer properties compared to **RM**.

3.7. Dipole Moment (*D*). The dipole moment is vital for determining the crystallinity and solubility phases. Such characteristics play a vital role in explaining the polarizing property in the solution phase for excellent organic photovoltaic systems (OPVS).[54] The molecule with high D values and high planarity charges could be transported continuously in that molecule. Therefore, the molecules' crystallinity is increased to attain higher solubility in the polar solvents, resulting from the tight packing of the structural parts. The higher excellent value of the dipole moment, the higher crystallinity and solubility of the polar solvents, which becomes more convenient.[55] The molecules with negligible D values are mostly not soluble in polar solvents. This fact is not universal; however, the planarity of the molecule decides the reactivity toward solvents and charge mobility.[26] The calculated dipole moment values of all studied molecules in both phases are listed in Tables 7 and 8.

Table 8. Dipole Moment of RM and AM1−AM6 Molecules in Both Gas and Solvent Phases

molecules	D (gas phase)	D (solution phase)
RM	0.545123	0.906143
AM1	9.997370	11.920228
AM2	2.920384	3.763479
AM3	1.782227	2.595225
AM4	6.020482	7.498012
AM5	4.882932	5.450876
AM6	2.916510	3.773208

https://doi.org/10.1021/acsomega.3c05176
ACS Omega 2023, 8, 42492−42510

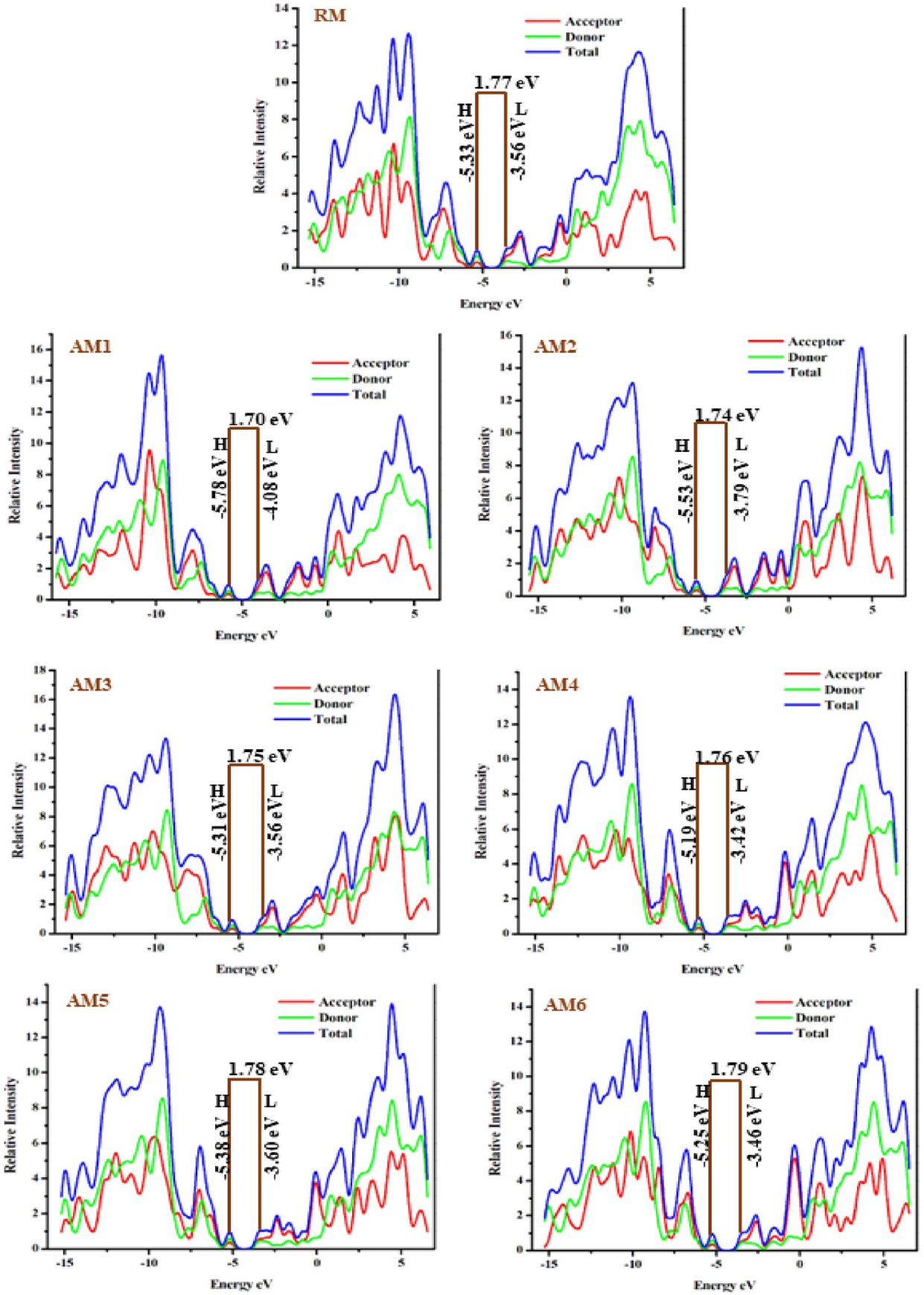

Figure 8. Dos graphs of **RM** and **AM1−AM6** molecules.

https://doi.org/10.1021/acsomega.3c05176
ACS Omega 2023, 8, 42492−42510

The decreasing value of the dipole moment is almost the same as that in the chloroform solvent phase, i.e., **AM1** > **AM4** > **AM5** > **AM6** > **AM2** > **AM3** > **RM**. It can be seen from the above trend that **the RM** molecule has the lowest value of the dipole moment. However, all the proposed molecules represented the higher value of dipole moment; therefore, all perceived molecules have high crystallinity and possess efficient abilities to be solubilized in chloroform solvent. Eventually, these molecules might be manufactured through solution-processed techniques.

3.8. Density of State Analysis. Density of state (DOS) analysis is significant in understanding how donor and acceptor parts of a molecule work collectively. The associated DOS, which may be either partial or total, establishes the complete potential of the molecule.[56] DOS analysis is essential for developing FMOs concerning Mulliken's charge density. The dos analysis of all the studied molecules was performed at a specified level of theory, and pyMolyze1.1 was utilized to design graphs and charts from the calculated data.[57] The DOS plots of all the studied molecules are shown in Figure 8, and the HOMO and LUMO contributions of each molecule are written in Table 9. In plots, the *x*-axis shows energy, and the *y*-axis represents the relative intensity of the molecule. The peaks above the negative values depict HOMO energy on the left side, and the central line shows the band gap (E_g). However, peaks above the positive values on the right side represent the LUMO energy. Separating each molecule's donor and acceptor (D/A) moieties helped us examine these subunits' effect on the FMOs.[58]

Table 9. Donors and Acceptors Contributions in the FMOs of RM and AM1−AM6 Molecules

molecules	excitation energy state	percentage contribution of donor(eV)	percentage contribution of acceptor(eV)
RM	HOMO	68.4	31.6
	LUMO	38.0	62.0
AM1	HOMO	60.7	39.3
	LUMO	43.3	56.7
AM2	HOMO	61.3	38.7
	LUMO	44.5	55.5
AM3	HOMO	61.3	38.7
	LUMO	45.2	54.8
AM4	HOMO	61.5	38.5
	LUMO	45.5	54.5
AM5	HOMO	62.0	38.0
	LUMO	46.4	53.6
AM6	HOMO	62.4	37.6
	LUMO	46.7	53.3

In the DOS plots of **RM** and all the designed molecules **AM1−AM6**, the red and green lines show the acceptor and donor participation in the FMOs. It can be concluded from the quantitative participation of each component that the central core part has almost 60% contribution in the HOMO region, and the end group acceptor has almost 39% participation in the LUMO region of all the examined molecules. This provides undeniable proof that the feasibility of charge mobility can be enhanced by continuous conjugation between donor and acceptor parts of a molecule, increasing the efficiency of organic solar cells. The planar structure of these investigated molecules resulted in the practical transportation from the e-rich core (donor) to the end group acceptors in an excited state, as represented by the results. In **AM1** and **AM6** molecules, acceptors have 56 and 62% contributions in the LUMO region of these molecules. The higher contribution in LUMO leads toward the stability of the LUMO region. Therefore, sable LUMO represents the greater extent of charge transfer from the donor to the acceptor region of the molecule.

3.9. Molecular Electrostatic Potential. The 3-D arrangement of an electronic cloud present on the atoms within a molecule is called the molecular electrostatic potential. It helps better investigate parts of a molecule with low and high electron density, elaborating electronic clouds of different colors.[59] The MEP structures of all of the studied molecules are shown in Figure 9. Here, the red and yellow hues represent the regions of high electron density, and the blue color shows the regions having low electron density. The blue and red areas of the molecule also represent the reactive nature of the molecule. The blue regions are good sites for electrophile attack, while the red areas are suitable for nucleophile attack due to their low and high electronic density.[60,61]

However, the blue part represents the positive potential for the donor (core), and the red part represents the negative potential for the terminal acceptor part of a molecule. The distinct blue and red hues show prominent charge separation in the molecules.[32,62] In the **RM** and all of the examined molecules **AM1−AM6**, the higher electron density is present on the oxygen and nitrogen atoms in the end-grouped acceptors. At the same time, the blue color is present on the methyl groups and thiophene rings of the donor regions due to their low electron density. Moreover, **AM5** exhibits the maximum positive and negative potential values of $+5.418 \times 10^{-2}$ and -5.418×10^{-2}, respectively, compared to all examined molecules.

3.10. Transition Density Matrix and Exciton Binding Energy Evaluation. Transition density matrix (TDM) evaluation is critical for precisely predicting electronic flux between acceptor and donor regions of π-conjugated geometries at specific sites.[63] This method allows for the prediction of charge transmissions, enormous charge regions, the direction of exciton motions during emissions, and absorption in the excited state.[64] TDM plots are mapped to examine the electronic properties, such as resonance influence, extent of delocalization, and how charges travel inside the molecule. The TDM graphs in Figure 10 were plotted using Multiwfn 3.7 software and the development of 2-D plots; for a better understanding of charge density, each plot is divided into donor and acceptor parts. Both the *x*-axis and the *y*-axis represent the bright fringes of the molecules without hydrogen atoms present in them. Hydrogen atoms are disfavored due to their negligible influence on electrostatic interactions.[61] The gradient bar on the right side of TDM plots shows charge density from zero electronic (blue) to high electronic (red) density.[65]

It can be seen from TDM graphs that a prominent off-diagonal charge density is present and diagonal in **RM** and all of the examined molecules (**AM1−AM6**). These pictures demonstrated the systematic conjugation of an end-group acceptor with a central core, elaborating the sequential transition of electrons from the donor to the acceptor part of the molecules. The **AM1** molecule has an efficient charge density distribution from the central core to the terminal accept region.

Exciton binding energy (E_b) is the minimum energy required to split a bounded electron and hole pair acquired

https://doi.org/10.1021/acsomega.3c05176
ACS Omega 2023, 8, 42492−42510

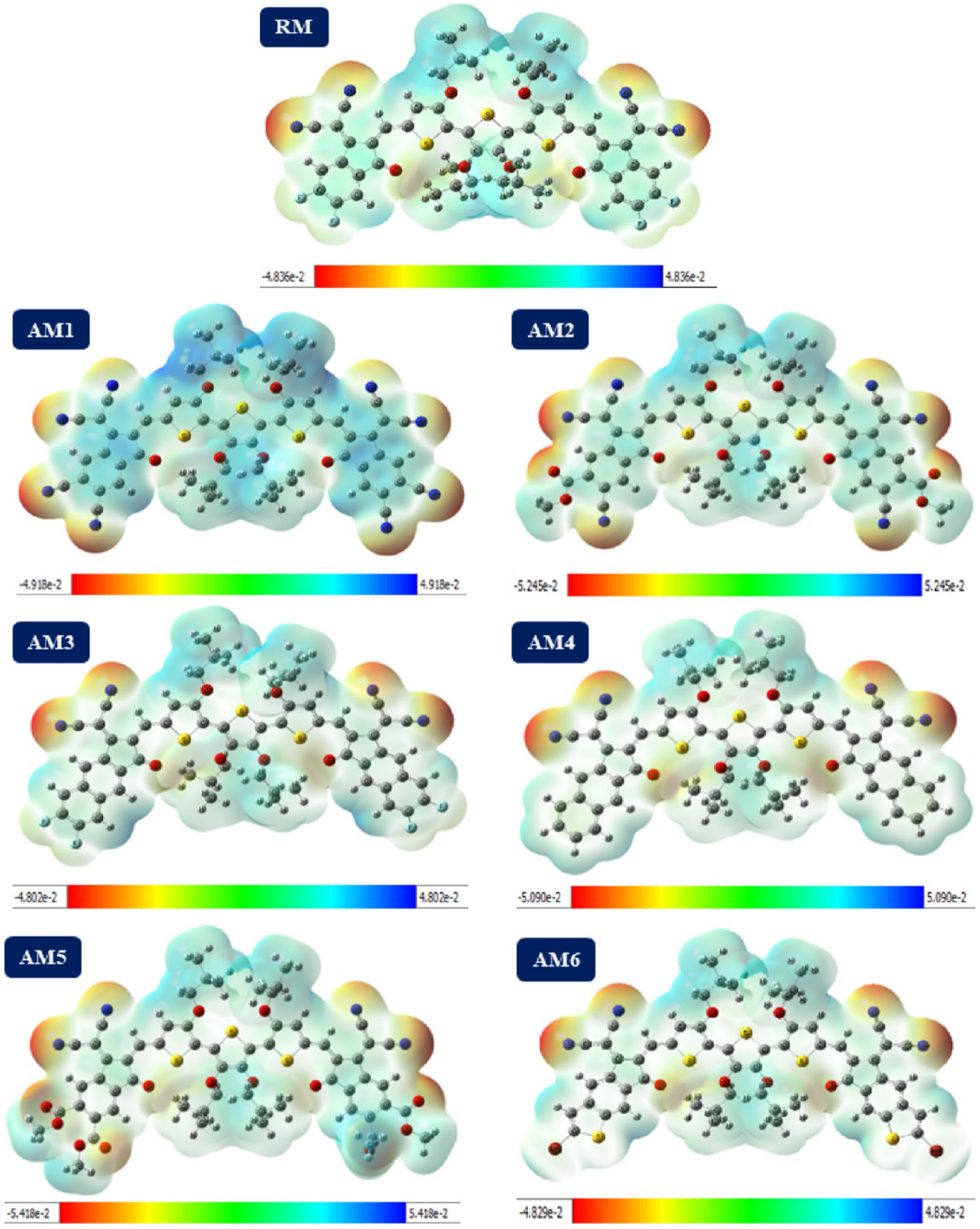

Figure 9. ESP structures of the **R** and **AM1**−**AM6** molecules.

by the absorption of radiation by a chromophore in OSCs. The more negligible the E_b value, the greater the exciton disintegration, thus more excellent electricity production, leading to the greater efficiency of the concerned organic photovoltaics (OPVs).[66] So, coulombic interactions develop in a molecule with low E_b; thus, fewer e-hole pairs are formed. Eventually, exciton dissociates readily with less E_b energy and quickly moves toward their concerned electrodes to produce electricity. The values of E_b can be calculated using the following eq 8.[67]

$$E_b = E_g - E_x \tag{8}$$

Here, E_g demonstrates the calculated band gap values of the molecules, and E_x represents the first excitation energy of the molecules.[68] The determined E_b values of RM and all the perceived molecules in both solvents are written in Table 10.

The E_b of all of the studied molecules in the gaseous state is increasing as **RM** = **AM1** = **AM2** < **AM3** = **AM4** = **AM5** < **AM6**. All of the molecules have comparable E_b values in comparison to the **RM** molecule. However, the decreasing E_b values of all analyzed molecules in the chloroform solvent are **RM** > **AM2** = **AM5** = **AM6** > **AM1** = **AM3** > **AM4**. All the molecules represent lower E_b values as compared to **RM** molecules. The **AM4** molecule has the lowest E_b value and

https://doi.org/10.1021/acsomega.3c05176
ACS Omega 2023, 8, 42492−42510

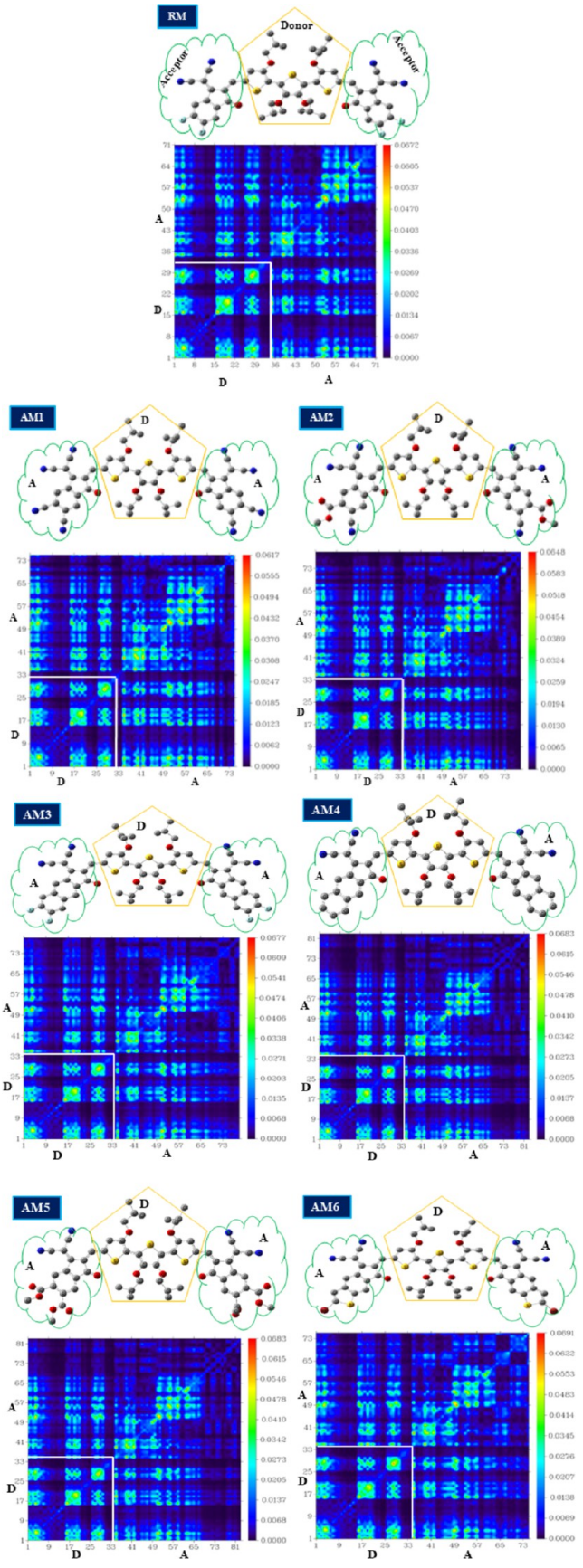

Figure 10. TDM plots of **RM** and **AM1−AM6** molecules.

Table 10. Energy Gap (E_{H-L}), E_b in Both Phases, and Interaction Coefficient of All of the Examined Molecules

molecules	E_{H-L} (eV)	E_b (eV) gaseous	E_b (eV) solvent	interaction coefficient
RM	1.77	0.09	0.32	0.70658
AM1	1.70	0.09	0.25	0.70526
AM2	1.74	0.09	0.26	0.70576
AM3	1.75	0.10	0.25	0.70592
AM4	1.76	0.10	0.24	0.70572
AM5	1.78	0.10	0.26	0.70619
AM6	1.79	0.11	0.26	0.70544

thus exhibits better charge transfer abilities among the other perceived molecules.

3.11. Reduced Density Gradient Evaluation. The noncovalent interactions (NCI) investigation is done with a 2D reduced density gradient graph (RDG), which is mainly concerned with NCI between the molecules and elaborates on hydrogen bonds and weak van der wall and stearic interactions. The Multiwfn program was utilized to develop scatter plots of RM and all proposed molecules (**AM1−AM6**). During the investigation, the nature of NCI λ_2 values is considered. For attractive interactions, $\lambda_2 < 0$, and for repulsive interactions, $\lambda_2 > 0$ was used. It can be visualized from Figure 11 that the hydrogen bonding and solid and attractive interactions are shown by blue color, the van der Waals interactions are elaborated by the green color, and repulsive solid interactions and the stearic effect are indicated by red color.

It can be seen from graphs that spikes on the left and right sides are more connected to positive and negative signs, thus exhibiting the highest positive and negative values of −0.05 and +0.05, respectively. The high stability of a molecule is due to low stearic hindrance and a potent H-bond combination. In **AM3** molecules, a greater extent of H-bonding is present with this molecule's oxygen and nitrogen atoms, as represented by a broader blue spike. Eventually, in all of the studied molecules, the extent of van der Wall forces is defined by the green spike region of each scatterplot. In **AM2**, **AM3**, and **AM6**, there is a greater extent of stearic interactions present in these molecules, as shown by a red spike of scatterplots.

Furthermore, isosurface analysis provides essential information about interactions between different fragments of a molecule. These intramolecular aggregations are represented by blue, green, and red discs. It can be observed that the red-colored spots are present inside the molecular rings in Figure 11. Green color, which represent attractive forces, is mostly present between hydrogen and corresponding electronegative atoms. These attractive forces are essential for maintaining the stability of molecules.

3.12. Reorganization Energy. Reorganization energy also has a prominent effect on the efficiency of OSCs. It helps analyze the extent of the charge carrier's mobility in the molecules.[69] Charge carrier movement (electron and hole mobility) has an inverse relationship to the RE of a molecule. Therefore, the lower RE value of a molecule can acquire higher electron (λ_-) and hole (λ_+) mobility. The geometrical structure of cations and anions is one of several properties that might influence the RE.[70] The calculated RE values of all the analyzed molecules are displayed in Table 11. These studies show that RE properties resemble the planarity of the scrutinized molecule.

https://doi.org/10.1021/acsomega.3c05176
ACS Omega 2023, 8, 42492−42510

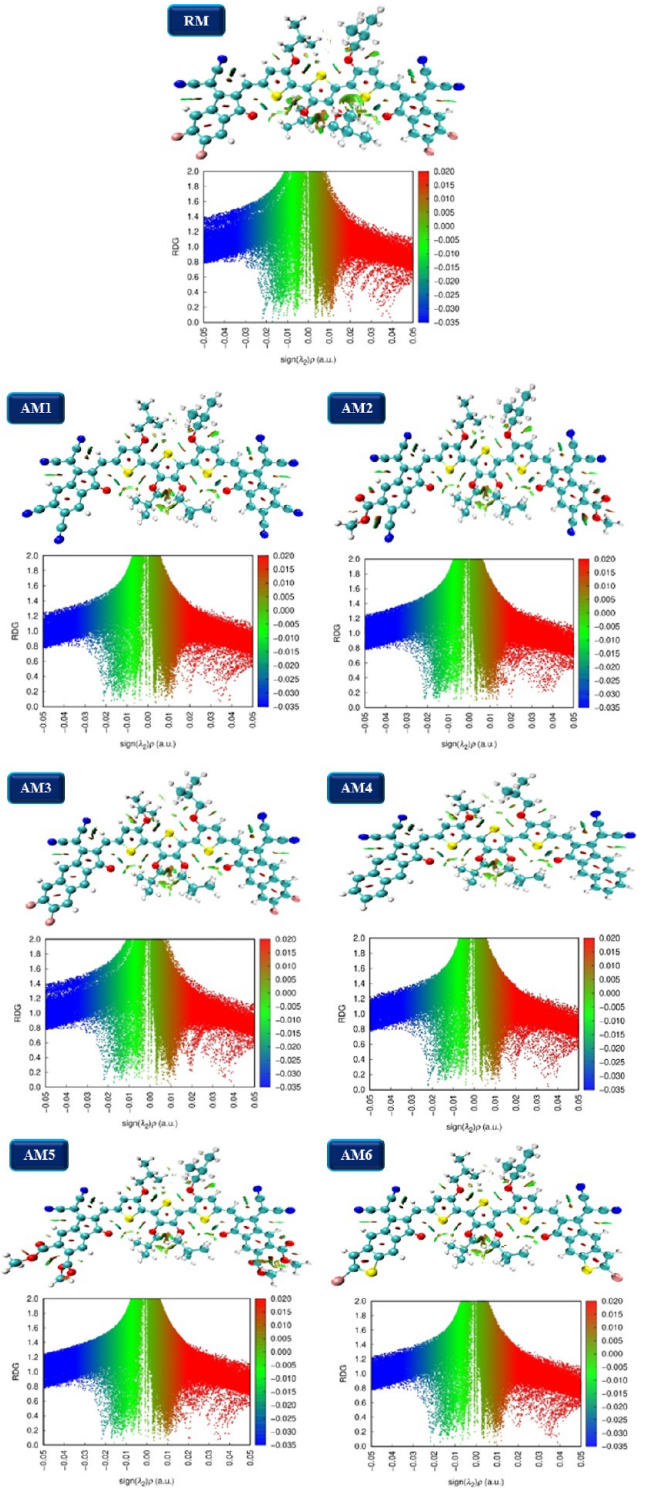

Figure 11. RDG plots of **RM** and **AM1**−**AM6** molecules.

It can be concluded from the tabulated data that the decreasing trend of λ_- is as **AM5** > **RM** > **AM6** > **AM3** > **AM4** > **AM2** > **AM1**. This means that all of the designed molecules are suitable electron transport materials due to lower RE values than the reference, except the **AM5** molecule. The fine morphology and planar structure of these molecules resulted in better exciton disintegration and the mobility of electrons. **AM1** has the lowest RE value (0.0062034 eV) for e−; thus, this molecule can be considered an efficient electron transport material in OSCs.

Table 11. Reorganization Energy for Electron (λ_-) and Hole (λ_+) for RM and AM1−AM6

molecules	electron (λ_-)	hole (λ_+)
RM	0.0082016	0.0091482
AM1	0.0062034	0.0086828
AM2	0.0071979	0.0082946
AM3	0.0072743	0.0089122
AM4	0.0072339	0.0087511
AM5	0.0083703	0.0097739
AM6	0.0080383	0.0090521

However, in the case of RE values for holes, the same trend is observed as in the case of electron values. Thus, **AM5** is not a much better hole-transporting material due to its high hole values compared to the **RM** molecule. While all other molecules also exhibit good λ_+ transporting properties, **AM1** and **AM2** are considered the most promising molecules in their respective photovoltaic cells and could pave the way toward NFSMAs based on efficient organic solar cells.

3.13. Open Circuit Voltage Assessment. V_{oc} is an essential parameter due to its direct relationship with OSCs' percentage conversion efficiency (PCE). It can be demonstrated that the highest voltage value produced when the current's availability across the system is nearly equal to zero is called V_{oc}.[32] It involved the conversion of photons into electrons. The below eq 9 was utilized to calculate the value of V_{oc}.

$$\boldsymbol{V}_{\mathrm{OC}} = \frac{1}{\mathbf{e}}(\boldsymbol{E}_{\mathbf{LUMO\ of\ acceptor}} - \boldsymbol{E}_{\mathbf{HOMO\ of\ donor}}) - 0.3 \tag{9}$$

Here, $E_{\mathrm{LUMO\ of\ acceptor}}$ is a HOMO of well-known polymer PTB7-Th that exhibits HOMO values −5.20 eV, and $E_{\mathrm{LUMO\ of\ acceptor}}$ is the LUMO value of our scrutinized molecule considered as acceptor, e is the molecule's charge sign, having a value of 1, and the 0.30 value is related to the coefficient of charges among the surfaces.[71,72] This polymer was selected because it exhibits LUMO values comparable to those of NFAs for convenient charge transfer. The most excellent voltage is produced when HOMO from the donor and LUMO from the acceptors are connected. Decreased HOMO and increased LUMO energies are required to attain enhanced Voc of perceived molecules, as shown in Table 11 and Figure 12. It can be seen that the computationally calculated V_{oc} value of our **RM** molecule was (1.34 eV), and the raising pattern of our designed molecules is **AM1** < **AM2** < **AM4** < **AM5** = **RM** < **AM6** < **AM3**. Although the efficient electron withdrawing group is present, the low V_{oc} values of **AM1**, **AM2**, and **AM4** might be due to low-lying LUMO compared to the HOMO of PTB7-Th. Therefore, these molecules might be used in efficient OSCs. The fill factor (FF) is an essential parameter in examining the PCE of photovoltaic systems. The donor's and acceptor's interface, V_{oc}, majorly affects the FF. The FF value of RM and all the proposed molecules were calculated by eq 10.[73]

$$\mathbf{FF} = \frac{\frac{\boldsymbol{eV}_{\mathrm{OC}}}{\boldsymbol{K}_{\mathrm{B}}\boldsymbol{T}} - \ln\left(\frac{\boldsymbol{eV}_{\mathrm{OC}}}{\boldsymbol{K}_{\mathrm{B}}\boldsymbol{T}} + 0.72\right)}{\frac{\boldsymbol{eV}_{\mathrm{OC}}}{\boldsymbol{K}_{\mathrm{B}}\boldsymbol{T}} + 1} \tag{10}$$

https://doi.org/10.1021/acsomega.3c05176
ACS Omega 2023, 8, 42492−42510

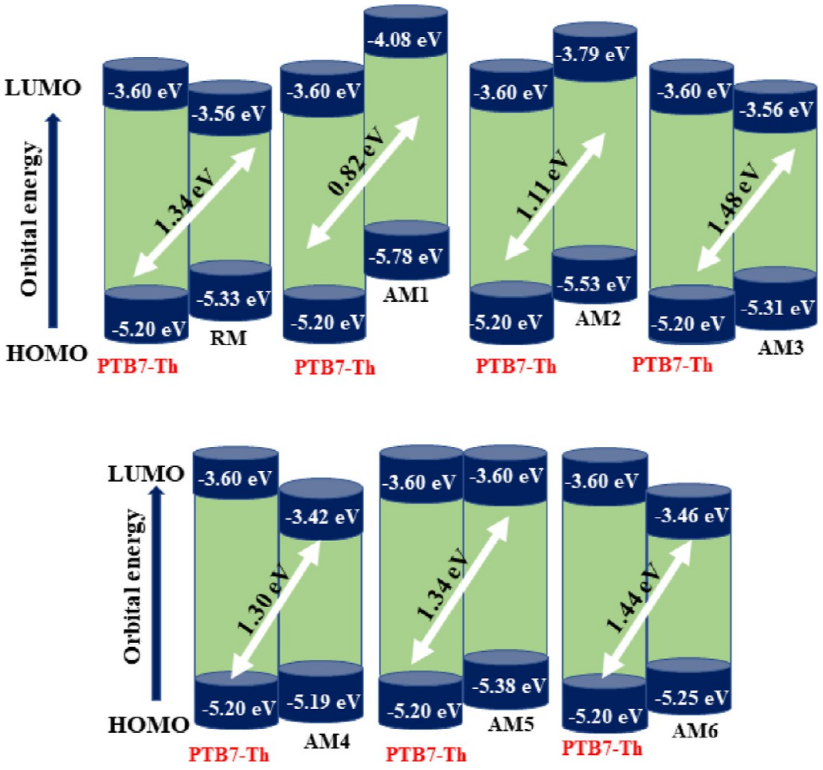

Figure 12. V_{oc} of **RM** and **AM1−AM6** acceptors along with the **PTB7-Th** donor.

Where eV_{oc} K_BT is the normalized V_{oc}, while e is the average charge having a value of 1, *KB* is the Boltzmann constant, and *T* represents temperature, a value up to 300 K. The concluded results revealed that **AM3** and **AM6** molecules represent higher normalized V_{oc} values (57.1981 and 55.6522 eV, respectively) than **RM** molecule values (51.7874 eV). Moreover, these molecules' computationally calculated FF values are also greater than those of **RM** molecules. However, these molecules have greater values than experimental ones. Thus, these can give an appropriate analysis of the investigation of those molecules having higher experimental FF values (although lower than theoretical values) than the other molecules.

Energy loss (E_{loss}) is also a necessary factor that significantly affects the functional behavior of OSCs. The extent of sunlight energy converted to electrical power directly relates to the amount of energy produced by organic solar cells. To a greater extent, energy loss resulted in a decline in the PCE value of OSCs. The PCE value also determines the amount of radiated energy converted to electricity. Producing OSCs with reduced E_{loss} values is a big challenge.[74] E_{loss} values of all studied molecules were calculated by eq 11 and tabulated in Table 12.

$$E_{loss} = E_g - qV_{oc} \tag{11}$$

Here, E_g elaborates on the FMOs gap, and q shows the charge of the element. The determined E_{loss} values of **RM** and all novel chromophores (**AM1−AM6**) are given in Table 12. The declining pattern of E_{loss} is as follows: **AM1** (0.88 eV) > **AM2** (0.63 eV) > **AM4** (0.46 eV) > **AM5** (0.44 eV) > **RM** (0.44 eV) > **AM6** (0.35 eV) > **AM3** (0.27 eV). The above pattern shows that **AM6** and **AM3** molecules exhibit less value than **RM**. Therefore, these molecules have efficient functional abilities among all examined chromophores due to reduced E_{loss} values; consequently, these are excellent molecules.

Table 12. V_{oc}, Normalized V_{oc}, and FF Values of RM and AM1−AM6 Molecules

molecules	V_{oc} (eV)	normalized V_{oc}	FF	energy loss (eV)
RM	1.34	51.7874	0.9060	0.43
AM1	0.82	31.6908	0.8630	0.88
AM2	1.11	42.8986	0.8912	0.63
AM3	1.48	57.1981	0.9131	0.27
AM4	1.30	50.2415	0.9038	0.46
AM5	1.34	51.7874	0.9060	0.44
AM6	1.44	55.6522	0.9112	0.35

PCE is calculated to investigate whether the PV properties of a molecule are fruitful for practical purposes and involve relevant factors of solar equipment working as a single unit. The PCE of the molecules is majorly affected by V_{oc}, J_{sc}, and FF. The relationship between these parameters can be visualized by eq 12.[75]

$$\mathbf{PCE} = \frac{J_{sc}V_{oc}\mathbf{FF}}{P_{in}} \tag{12}$$

Using the above formulas, we computed the V_{oc}, normalized V_{oc}, and FF values of **RM** and all proposed molecules **AM1−AM6**. In contrast, the J_{sc} value was not calculated due to their limited capabilities. It has been represented previously that LHE is one of the parameters used to determine J_{sc}. The **AM3** and **AM6** molecules might represent greater PCE than the RM molecules, as expected by the higher V_{oc} and FF values of these molecules.

3.14. Charge Transfer at Donor/Acceptor Interface Validation. The NTOs analysis was performed to confirm the charge transfer efficiency and compare the molecular frameworks of the donor and acceptor for interface development. The literature study has explored that for excellent charge

https://doi.org/10.1021/acsomega.3c05176
ACS Omega 2023, 8, 42492−42510

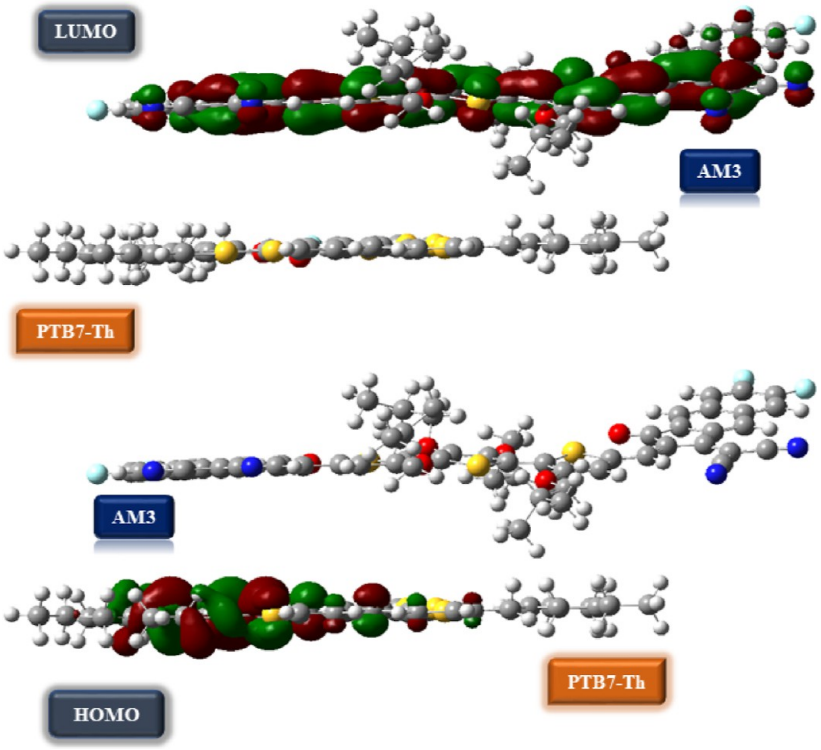

Figure 13. HOMO/LUMO structures of **PTB7-Th** along with the **AM3** molecule.

transfer at the D/A interface, there must be high planarity, HOMO charge density on the donor region, and LUMO charge density on the acceptor region of the molecule.[76] The obtained results from the selected D/A interface PTB7-Th AM3 show that our utilized polymer acting as HOMO (donor) and our perceived molecule acting as LUMO (acceptor) are revealed by the charge density on both molecules. The HOMO−LUMO charge density is represented in Figure 13. The highest planarity of both molecules validated them as excellent molecules for charge transfer at the interface because planarity enabled them to achieve higher crystallinity and closer packing.

3.15. Charge Transfer at Donor/Acceptor Interface Validation. The NTOs analysis was performed to confirm the charge transfer efficiency and compare the molecular frameworks of the donor and acceptor for interface development. The literature study has explored that for excellent charge transfer at the D/A interface, there must be high planarity, HOMO charge density on the donor region, and LUMO charge density on the acceptor region of the molecule.[76] The obtained results from the selected D/A interface PTB7-Th AM3 show that our utilized polymer acting as HOMO (donor) and our perceived molecule acting as LUMO (acceptor) are revealed by the charge density on both molecules. The HOMO−LUMO charge density is represented in Figure 13. The highest planarity of both molecules validated them as excellent molecules for charge transfer at the interface because planarity enabled them to achieve higher crystallinity and closer packing.

4. CONCLUSIONS

In this study, nonfullerene acceptor-based six A−D−A type molecules (**AM1**−**AM6**) were computationally designed to improve the OSCs performance by substituting the end group acceptors of the **RM** molecule. The reduced band gap of **AM1**, **AM2**, **AM3**, and **AM4** compared the **RM** suggests an improved probability of charge transfer in these designed molecules. Furthermore, the band gap also affects the absorption of molecules. It can be seen that the λ_{max} of almost all molecules is higher than RM. This shows that these newly designed molecules are more capable of absorbing light energy, as evidenced by their improved LHE values. Regarding charge mobility, different crucial parameters were evaluated. Except **AM5**, all other newly designed molecules represented lower RE values for the electron (λ_{-}), representing greater electron mobility than **RM** (0.0082016). Remarkably, **AM2** represented the most negligible RE value (0.0082946) for the hole (λ_{+}) from all of the examined molecules, exhibiting the highest λ_{+} mobility for this molecule. The **AM1**−**AM6** molecules have greater dipole moment values, which can improve their crystallinity, solubility, and charge transfer. The donor polymer PTB7-Th was coupled to the NFSMAs to verify the probability of charge transfer. **AM3** (1.48 eV) and **AM6** (1.44 eV) represented higher V_{oc} values and reduced E_{loss} values than the **RM** (1.34 eV). So, based on these results, it can be estimated that **AM3** and **AM6** are more favorable to yield greater PCEs. Overall, the analysis of different photovoltaic parameters revealed that all structured molecules could produce efficient OSCs with extraordinary photovoltaic properties.

■ ASSOCIATED CONTENT

Supporting Information

The Supporting Information is available free of charge at https://pubs.acs.org/doi/10.1021/acsomega.3c05176.

Detailed Cartesian coordinates of internally optimized geometries of studied molecules (PDF)

https://doi.org/10.1021/acsomega.3c05176
ACS Omega 2023, 8, 42492−42510

AUTHOR INFORMATION

Corresponding Authors

Rasheed Ahmad Khera − *Department of Chemistry, University of Agriculture, Faisalabad 38000, Pakistan;* orcid.org/0000-0002-5513-8096; Email: rasheedahmadkhera@yahoo.com, rasheed.ahmad.khera@uaf.edu.pk

Mohamed Shaban − *Department of Physics, Faculty of Science, Islamic University of Madinah, Madinah 42351, Saudi Arabia;* orcid.org/0000-0002-4368-8269; Email: mssfadel@aucegypt.edu

Muhammad Waqas − *Department of Chemistry, University of Agriculture, Faisalabad 38000, Pakistan;* orcid.org/0000-0002-2446-6740; Email: muhammadwaqas1005@gmail.com

Authors

Faseh Ur Rehman − *Department of Chemistry, University of Agriculture, Faisalabad 38000, Pakistan*

Shanza Hameed − *Department of Chemistry, University of Agriculture, Faisalabad 38000, Pakistan*

Manel Essid − *Chemistry Department, College of Science, King Khalid University (KKU), Abha 9004, Saudi Arabia*

Zouhaier Aloui − *Chemistry Department, College of Science, King Khalid University (KKU), Abha 9004, Saudi Arabia*

Sameerah I. Al-Saeedi − *Department of Chemistry. Collage of Science, Princess Nourah Bint Abdulrahman University, Riyadh 11671, Saudi Arabia*

Mahmoud A. A. Ibrahim − *Chemistry Department, Faculty of Science, Minia University, Minia 61519, Egypt; School of Health Sciences, University of KwaZulu-Natal, Durban 4000, South Africa;* orcid.org/0000-0003-4819-2040

Complete contact information is available at: https://pubs.acs.org/10.1021/acsomega.3c05176

Notes

The authors declare no competing financial interest.

ACKNOWLEDGMENTS

The authors extend their appreciation to the Deanship of Scientific Research at King Khalid University for funding this work through large group Research Project under grant number RGP2/110/44.

REFERENCES

(1) Rahman, A.; Farrok, O.; Haque, M. M. Environmental impact of renewable energy source based electrical power plants: Solar, wind, hydroelectric, biomass, geothermal, tidal, ocean, and osmotic. *Renew. Sustain. Energy Rev.* **2022**, *161*, 112279.

(2) Wang, X. Embedded Host/Guest Alloy Aggregations Enable High-Performance Ternary Organic Photovoltaics. *Adv. Mater.* **2023**, 2305652.

(3) Li, S.; Li, Z.; Wan, X.; Chen, Y. Recent progress in flexible organic solar cells. *eScience* **2023**, *3*, 100085.

(4) Subudhi, P.; Punetha, D. Progress, challenges, and perspectives on polymer substrates for emerging flexible solar cells: A holistic panoramic review. *Prog. Photovolt.: Res. Appl.* **2023**, *31* (8), 753−789.

(5) Bai, Y.; Zhang, Z.; Zhou, Q.; Geng, H.; Chen, Q.; Kim, S.; Zhang, R.; Zhang, C.; Chang, B.; Li, S.; et al. Geometry design of tethered small-molecule acceptor enables highly stable and efficient polymer solar cells. *Nat. Commun.* **2023**, *14* (1), 2926.

(6) Han, C.; Wang, J.; Zhang, S.; Chen, L.; Bi, F.; Wang, J.; Yang, C.; Wang, P.; Li, Y.; Bao, X. Over 19% Efficiency Organic Solar Cells by Regulating Multidimensional Intermolecular Interactions. *Adv. Mater.* **2023**, *35* (10), 2208986.

(7) Cao, J.; Du, F.; Yang, L.; Tang, W. The design of dithieno [3, 2-b: 2′, 3′-d] pyrrole organic photovoltaic materials for high-efficiency organic/perovskite solar cells. *J. Mater. Chem. A* **2020**, *8* (43), 22572−22592.

(8) Rani, S.; Al-Zaqri, N.; Iqbal, J.; Akram, S. J.; Boshaala, A.; Mehmood, R. F.; Saeed, M. U.; Rashid, E. U.; Khera, R. A. Designing dibenzosilole core based, A 2-π-A 1-π-D-π-A 1-π-A 2 type donor molecules for promising photovoltaic parameters in organic photovoltaic cells. *RSC Adv.* **2022**, *12* (45), 29300−29318.

(9) Yao, Z.; Li, Y.; Li, S.; Xiang, J.; Xia, X.; Lu, X.; Shi, M.; Chen, H. conformation locking of simple nonfused electron acceptors via multiple intramolecular noncovalent bonds to improve the performances of organic solar cells. *ACS Appl. Energy Mater.* **2020**, *4* (1), 819−827.

(10) Rashid, E. U.; Iqbal, J.; Khan, M. I.; El-Badry, Y. A.; Ayub, K.; Khera, R. A. Synergistic end-capped engineering on nonfused thiophene ring-based acceptors to enhance the photovoltaic properties of organic solar cells. *RSC Adv.* **2022**, *12* (20), 12321−12334.

(11) Akram, M.; Siddique, S. A.; Iqbal, J.; Hussain, R.; Mehboob, M. Y.; Siddique, M. B. A.; Naveed, S.; Ali, B.; Hanif, A.; Sajid, M.; et al. End-capped engineering of bipolar diketopyrrolopyrrole based small electron acceptor molecules for high performance organic solar cells. *Comput. Theor. Chem.* **2021**, *1201*, 113242.

(12) Siddique, S. A.; Arshad, M.; Naveed, S.; Mehboob, M. Y.; Adnan, M.; Hussain, R.; Ali, B.; Siddique, M. B. A.; Liu, X. Efficient tuning of zinc phthalocyanine-based dyes for dye-sensitized solar cells: a detailed DFT study. *RSC Adv.* **2021**, *11* (44), 27570−27582.

(13) Siddique, S. A.; Naveed, S.; Alvi, M. U.; Mehboob, M. Y.; Ali, B.; Rauf, A.; Siddique, M. B. A.; Hussain, R.; Arshad, M.; Liu, X. Deciphering the role of end-capped acceptor units for amplifying the photovoltaic properties of donor materials for high-performance organic solar cell applications. *Comput. Theor. Chem.* **2021**, *1205*, 113454.

(14) Janjua, M. R. S. A. All-small-molecule organic solar cells with high fill factor and enhanced open-circuit voltage with 18.25% PCE: Physical insights from quantum chemical calculations. *Spectrochim. Acta, Part A* **2022**, *279*, 121487.

(15) Khan, J. I.; Alamoudi, M. A.; Chaturvedi, N.; Ashraf, R. S.; Nabi, M. N.; Markina, A.; Liu, W.; Dela Peña, T. A.; Zhang, W.; Alévêque, O.; et al. Impact of Acceptor Quadrupole Moment on Charge Generation and Recombination in Blends of IDT Based Non Fullerene Acceptors with PCE10 as Donor Polymer. *Adv. Energy Mater.* **2021**, *11* (28), 2100839.

(16) Ming, R.; Zhang, M.; Gao, W.; Ning, W.; Luo, Z.; Zhong, C.; Zhang, F.; Yang, C. Fluorene-fused ladder-type non-fullerene small molecule acceptors for high-performance polymer solar cells. *Mater. Chem. Front.* **2019**, *3* (4), 709−715.

(17) Kan, B.; Kan, Y.; Zuo, L.; Shi, X.; Gao, K. Recent progress on all-small molecule organic solar cells using small-molecule nonfullerene acceptors. *InfoMat* **2021**, *3* (2), 175−200.

(18) Waqas, M.; Iqbal, J.; Mehmood, R. F.; Akram, S. J.; Shawky, A. M.; Raheel, M.; Rashid, E. U.; Khera, R. A. impact of end-capped modification of MO-IDT based non-fullerene small molecule acceptors to improve the photovoltaic properties of organic solar cells. *J. Mol. Graph. Model.* **2022**, *116*, 108255.

(19) Mumit, M. A.; Pal, T. K.; Alam, M. A.; Islam, M. A. A. A. A.; Paul, S.; Sheikh, M. C. DFT studies on vibrational and electronic spectra, HOMO-LUMO, MEP, HOMA, NBO and molecular docking analysis of benzyl-3-N-(2, 4, 5-trimethoxyphenylmethylene) hydrazinecarbodithioate. *J. Mol. Struct.* **2020**, *1220*, 128715.

(20) Dege, N.; Gökce, H.; Doğan, O. E.; Alpaslan, G.; Ağar, T.; Muthu, S.; Sert, Y. Quantum computational, spectroscopic investigations on N-(2-((2-chloro-4, 5-dicyanophenyl) amino) ethyl)-4-methylbenzenesulfonamide by DFT/TD-DFT with different solvents, molecular docking and drug-likeness researches. *Colloids Surf., A* **2022**, *638*, 128311.

(21) Waqas, M.; Hadia, N.; Hessien, M.; Iqbal, J.; Mersal, G. A.; Hameed, S.; Shawky, A. M.; Aloui, Z.; Ibrahim, M. A.; Ahmad Khera, R. End-group modification of terminal acceptors on benzothiadiazole-based BT2F-IC4F molecule to establish efficient organic solar cells. *J. Mol. Liq.* **2022**, *368*, 120770.
(22) Zahid, S.; Rasool, A.; Zahid, S.; Ans, M.; Iqbal, J.; El Azab, I. H.; Mersal, G. A.; Ibrahim, M. M. Designing easily synthesizable nonfused small acceptors for organic solar cells. *Sol. Energy* **2022**, *246*, 23−35.
(23) Zhao, Y.; Pu, J.; Lynch, B. J.; Truhlar, D. G. Tests of second-generation and third-generation density functionals for thermochemical kineticsElectronic supplementary information (ESI) available: Mean errors for pure and hybrid DFT methods. See http://www.rsc.org/suppdata/cp/b3/b316260e/. *Phys. Chem. Chem. Phys.* **2004**, *6* (4), 673−676.
(24) Zhihong, Y.; Ye, Y.; Pejhan, A.; Nasr, A.; Nourbakhsh, N.; Tayebee, R. A theoretical study on the pure and doped ZnO nanoclusters as effective nanobiosensors for 5 fluorouracil anticancer drug adsorption. *Appl. Organomet. Chem.* **2020**, *34* (4), No. e5534.
(25) de Castilho, L. L.; dos Santos, F. E. B.; Baptista, L. Approach to evaluate the gas/aerosol partition coefficient of organic volatile compounds using DFT methods associated with polarizable continuum models. *Atmos. Environ.* **2020**, *224*, 117363.
(26) Zubair, I.; Ahmad Kher, R.; Javaid Akram, S.; El-Badry, Y. A.; Umar Saeed, M.; Iqbal, J. Tuning the optoelectronic properties of indacenodithiophene based derivatives for efficient photovoltaic applications: a DFT approach. *Chem. Phys. Lett.* **2022**, *793*, 139459.
(27) Ajmal, M.; Ali, U.; Javed, A.; Tariq, A.; Arif, Z.; Iqbal, J.; Shoaib, M.; Ahmed, T. Designing indaceno thiophene-based three new molecules containing non-fullerene acceptors as strong electron withdrawing groups with DFT approaches. *J. Mol. Model.* **2019**, *25*, 311−319.
(28) Akram, S. J.; Hadia, N. M. A.; Shawky, A. M.; Iqbal, J.; Khan, M. I.; Alatawi, N. S.; Ibrahim, M. A. A.; Ans, M.; Khera, R. A. Designing of Thiophene [3, 2-b] Pyrrole Ring-Based NFAs for High-Performance Electron Transport Materials: A DFT Study. *ACS Omega* **2023**, *8* (12), 11118−11137.
(29) Mehboob, M. Y.; Khan, M. U.; Hussain, R.; Hussain, R.; Ayub, K.; Sattar, A.; Ahmad, M. K.; Irshad, Z.; Saira; Adnan, M. Designing of benzodithiophene core-based small molecular acceptors for efficient non-fullerene organic solar cells. *Spectrochim. Acta, Part A* **2021**, *244*, 118873.
(30) Swick, S. M.; Alzola, J. M.; Sangwan, V. K.; Amsterdam, S. H.; Zhu, W.; Jones, L. O.; Powers-Riggs, N.; Facchetti, A.; Kohlstedt, K. L.; Schatz, G. C.; et al. Fluorinating π Extended Molecular Acceptors Yields Highly Connected Crystal Structures and Low Reorganization Energies for Efficient Solar Cells. *Adv. Energy Mater.* **2020**, *10* (23), 2000635.
(31) ul Ain, Q.; Shehzad, R. A.; Yaqoob, U.; Sharif, A.; Sajid, Z.; Rafiq, S.; Iqbal, S.; Khalid, M.; Iqbal, J. Designing of benzodithiophene acridine based Donor materials with favorable photovoltaic parameters for efficient organic solar cell. *Comput. Theor. Chem.* **2021**, *1200*, 113238.
(32) Waqas, M.; Hadia, N.; Hessien, M.; Javaid Akram, S.; Shawky, A. M.; Iqbal, J.; Ibrahim, M. A.; Ahmad Khera, R. Designing of symmetrical ADA type non-fullerene acceptors by side-chain engineering of an indacenodithienothiophene (IDTT) core based molecule: a computational approach. *Comput. Theor. Chem.* **2022**, *1217*, 113904.
(33) Li, Q.; Li, Z. Molecular packing: another key point for the performance of organic and polymeric optoelectronic materials. *Acc. Chem. Res.* **2020**, *53* (4), 962−973.
(34) Majeed, M.; Waqas, M.; Mehmood, R. F.; Alatawi, N. S.; Essid, M.; Khera, R. A. Modified optoelectronic parameters by end-group engineering of ADA type non-fullerene-based small symmetric acceptors constituting IBDT core for high-performance photovoltaics. *J. Phys. Chem. Solids* **2023**, *181*, 111495.
(35) Sadiq, S.; Waqas, M.; Zahoor, A.; Mehmood, R. F.; Essid, M.; Aloui, Z.; Khera, R. A.; Akram, S. J. Synergistic modification of end groups in Quinoxaline fused core-based acceptor molecule to enhance its photovoltaic characteristics for superior organic solar cells. *J. Mol. Graph. Model.* **2023**, *123*, 108518.
(36) Maqsood, M. H.; Khera, R. A.; Mehmood, R. F.; Akram, S. J.; Al-Zaqri, N.; Ibrahim, M. A.; Noor, S.; Waqas, M. End-cap modeling on the thienyl-substituted benzodithiophene trimer-based donor molecule for achieving higher photovoltaic performance. *J. Mol. Graph. Model.* **2023**, *124*, 108550.
(37) Zahoor, A.; Hadia, N. M. A.; Akram, S. J.; Mehmood, R. F.; Sadiq, S.; Shawky, A. M.; Alatawi, N. S.; Ahmed, A.; Iqbal, J.; Khera, R. A. Alteration of the central core of a DF-PCIC chromophore to boost the photovoltaic applications of non-fullerene acceptor based organic solar cells. *RSC Adv.* **2023**, *13* (10), 6530−6547.
(38) Abdelkhalk, A.; Mustafa, C.; Siham, E. A.; Morad, E. B.; Benachir, E.; Mohammed, E. i.; Said, L. A computational study of thiophene containing small-molecule electron acceptors for non-fullerene organic photovoltaic cells. *Mater. Sci. Energy Technol.* **2023**, *6*, 137−144.
(39) Sumdani, M. G.; Islam, M. R.; Yahaya, A. N. A.; Safie, S. I. Recent advancements in synthesis, properties, and applications of conductive polymers for electrochemical energy storage devices: A review. *Polym. Eng. Sci.* **2022**, *62* (2), 269−303.
(40) Huang, X.; Oh, J.; Cheng, Y.; Huang, B.; Ding, S.; He, Q.; Wu, F.; Yang, C.; Chen, L.; Chen, Y. Narrow band-gap materials with overlapping absorption simultaneously increase the open circuit voltage and average visible transmittance of semitransparent organic solar cells. *J. Mater. Chem. A* **2021**, *9* (9), 5711−5719.
(41) Miar, M.; Shiroudi, A.; Pourshamsian, K.; Oliaey, A. R.; Hatamjafari, F. Theoretical investigations on the HOMO-LUMO gap and global reactivity descriptor studies, natural bond orbital, and nucleus-independent chemical shifts analyses of 3-phenylbenzo [d] thiazole-2 (3 H)-imine and its para-substituted derivatives: Solvent and substituent effects. *J. Chem. Res.* **2021**, *45* (1−2), 147−158.
(42) Haseena, S.; Ravva, M. K. Theoretical studies on donor-acceptor based macrocycles for organic solar cell applications. *Sci. Rep.* **2022**, *12* (1), 15043.
(43) Kshirsagar, B.; Jaykhedkar, N.; Jain, K.; Kishor, S.; Shah, V.; Ramaniah, L. M.; Tiwari, S. Green CsSnX3 (X= Cl, Br, I)-Derived Quantum Dots for Photovoltaic Applications: First-Principles Investigations. *J. Phys. Chem. C* **2021**, *125* (4), 2592−2606.
(44) Smalø, H.; Astrand, P.-O.; Ingebrigtsen, S. Calculation of ionization potentials and electron affinities for molecules relevant for streamer initiation and propagation. *IEEE Trans. Dielectr. Electr. Insul.* **2010**, *17* (3), 733−741.
(45) Sutradhar, T.; Misra, A. Enhancement of Nonlinear Optical Properties of Indole Based Dyes through Electron Acceptor and π Linker for Dye Sensitized Solar Cell Applications. *ChemistrySelect* **2019**, *4* (13), 3697−3705.
(46) Sabir, S.; Hadia, N.; Iqbal, J.; Mehmood, R. F.; Akram, S. J.; Khan, M. I.; Shawky, A. M.; Raheel, M.; Somaily, H.; Khera, R. A. DFT molecular modeling of A2-D-A1-D-A2 type DF-PCIC based small molecules acceptors for organic photovoltaic cells. *Chem. Phys. Lett.* **2022**, *806*, 140026.
(47) Naveed, A. Impact of end capped modification on BT-CIC molecule for high-performance photovoltaic attributes: a DFT approach. *J. Mol. Model.* **2022**, *28* (8), 218.
(48) Dua, H., Kaya, S., Sarkar, U., On the study of dye sensitized solar cells with high light harvesting efficiency and correlation of its chemical reactivity parameters with overall performance. **2023**..
(49) Fan, Q.; Ma, R.; Liu, T.; Su, W.; Peng, W.; Zhang, M.; Wang, Z.; Wen, X.; Cong, Z.; Luo, Z.; et al. 10.13% Efficiency All Polymer Solar Cells Enabled by Improving the Optical Absorption of Polymer Acceptors. *Sol. RRL* **2020**, *4* (6), 2000142.
(50) Rahmany, S.; Etgar, L. Semitransparent perovskite solar cells. *ACS Energy Lett.* **2020**, *5* (5), 1519−1531.
(51) Louis, H.; Eno, E. A.; Timothy, R. A.; Agwamba, E. C.; Unimuke, T. O.; Bukie, P. T.; Chukwudubem, I. E.; Offiong, O. E. Understanding the influence of alkyl-chains and hetero-atom (C, S, O) doped electron-acceptor fullerene-free benzothiazole for applica-

https://doi.org/10.1021/acsomega.3c05176
ACS Omega 2023, 8, 42492−42510

tion in organic solar cell: first principle perception. *Opt. Quant. Electron.* **2022**, *54* (11), 681.
(52) Afolabi, S. O.; Semire, B.; Akiode, O. K.; Idowu, M. A. Quantum study on the optoelectronic properties and chemical reactivity of phenoxazine-based organic photosensitizer for solar cell purposes. *Theor. Chem. Acc.* **2022**, *141* (4), 22.
(53) Saad Ebied, M.; Dongol, M.; Ibrahim, M.; Nassary, M.; Elnobi, S.; Abuelwafa, A. A. Effect of carboxylic acid and cyanoacrylic acid as anchoring groups on Coumarin 6 dye for dye-sensitized solar cells: DFT and TD-DFT study. *Struct. Chem.* **2022**, *33* (6), 1921−1933.
(54) Li, D.; Sun, C.; Yan, T.; Yuan, J.; Zou, Y. Asymmetric non-fullerene small-molecule acceptors toward high-performance organic solar cells. *ACS Cent. Sci.* **2021**, *7* (11), 1787−1797.
(55) Wang, P.; Li, Y.; Han, C.; Wang, J.; Bi, F.; Zheng, N.; Yang, J.; Wang, J.; Bao, X. Rationally regulating the π-bridge of small molecule acceptors for efficient organic solar cells. *J. Mater. Chem. A* **2022**, *10* (34), 17808−17816.
(56) Poduval, G. K.; Duan, L.; Hossain, M. A.; Sang, B.; Zhang, Y.; Zou, Y.; Uddin, A.; Hoex, B. High efficiency nonfullerene organic solar cells enabled by atomic layer deposited zirconium doped zinc oxide. *Sol. RRL* **2020**, *4* (10), 2000241.
(57) Mahalingavelar, P. How End-Capped Acceptors Regulate the Photovoltaic Performance of the Organic Solar Cells: A Detailed Density Functional Exploration of Their Impact on the A-D- π-D-A Type Small Molecular Electron Donors. *Energy Fuels* **2022**, *36* (4), 2095−2107.
(58) Waqas, M.; Hadia, N. M. A.; Shawky, A. M.; Mahmood, R. F.; Essid, M.; Aloui, Z.; Alatawi, N. S.; Iqbal, J.; Khera, R. A. Theoretical framework for achieving high V oc in nonfused non-fullerene terthiophene-based end-capped modified derivatives for potential applications in organic photovoltaics. *RSC Adv.* **2023**, *13* (11), 7535−7553.
(59) Fatima, A.; Khanum, G.; Agrawal, D. D.; Srivastava, S. K.; Butcher, R. J.; Muthu, S.; Ahmad, M.; Althubeiti, K.; Siddiqui, N.; Javed, S. Synthesis, Spectroscopic, Crystal Structure, DFT, Hirshfeld Surface and Molecular Docking Analysis of Hexahydroquinoline Derivative (HQ). *Polycyclic Aromat. Compd.* **2022**, *43*, 4242−4270.
(60) Zahoor, A.; Sadiq, S.; Khera, R. A.; Essid, M.; Aloui, Z.; Alatawi, N. S.; Ibrahim, M. A.; Hasanin, T. H.; Waqas, M. A DFT study for improving the photovoltaic performance of organic solar cells by designing symmetric non-fullerene acceptors by quantum chemical modification on pre-existed LC81 molecule. *J. Mol. Graph. Model.* **2023**, *125*, 108613.
(61) Ishtiaq, M.; Waqas, M.; Zubair, H.; Mehmood, R. F.; Al-Zaqri, N.; Khera, R. A.; Ibrahim, M. A.; Iqbal, J. Theoretical designing of symmetrical non-fullerene acceptor molecules by end-capped modification for promising photovoltaic properties of organic solar cells. *J. Mol. Liq.* **2023**, *386*, 122473.
(62) Celik, S. DFT investigations and molecular docking as potent inhibitors of SARS-CoV-2 main protease of 4-phenylpyrimidine. *J. Mol. Struct.* **2023**, *1277*, 134895.
(63) Malmqvist, P. . Å. Calculation of transition density matrices by nonunitary orbital transformations. *Int. J. Quant. Chem.* **1986**, *30* (4), 479−494.
(64) Luzanov, A.; Sukhorukov, A.; Umanskii, V. Application of transition density matrix for analysis of excited states. *Theor. Exp. Chem.* **1976**, *10*, 354−361.
(65) Khan, M. I.; Hadia, N.; Shawky, A. M.; Hessien, M.; Essid, M.; Akram, S. J.; Iqbal, J.; Alatawi, N. S.; Mersal, G. A.; Khera, R. A. Quantum mechanical modeling of fused rings-based small-donor molecules with enhanced optoelectronic attributes for high performance organic photovoltaic cells. *J. Phys. Chem. Solids* **2023**, *174*, 111140.
(66) Sandeep, S. Investigations of nonlinear optical effects and ultrafast laser Induced plasma in nanostructured media. Doctorate Thesis, 2012.
(67) Jiang, Z.; Lou, W.; Liu, Y.; Li, Y.; Song, H.; Chang, K.; Duan, W.; Zhang, S. Spin-triplet excitonic insulator: The case of semi-hydrogenated graphene. *Phys. Rev. Lett.* **2020**, *124* (16), 166401.
(68) Shuai, Z.; Li, W.; Ren, J.; Jiang, Y.; Geng, H. Applying Marcus theory to describe the carrier transports in organic semiconductors: Limitations and beyond. *J. Chem. Phys.* **2020**, *153* (8), 080902.
(69) Ullah Rashid, E.; Iqbal, J.; Farhat Mehmood, R.; El-Badry, Y. A.; Javaid Akram, S.; Ahmad Khera, R. Depicting the role of end-capped acceptors to amplify the photovoltaic properties of benzothiadiazole core-based molecules for high-performance organic solar cell applications. *Comput. Theor. Chem.* **2022**, *1211*, 113669.
(70) Cao, M.; Wang, L.; Gao, H.; Jiang, H.; Song, H. Intrinsic influence of selenium substitution in thiophene and benzo-2, 1, 3-thiadiazole on the electronic structure, excited states and photovoltaic performances evaluated using theoretical calculations. *New J. Chem.* **2023**, *47*, 1797−1807.
(71) Poelking, C.; Benduhn, J.; Spoltore, D.; Schwarze, M.; Roland, S.; Piersimoni, F.; Neher, D.; Leo, K.; Vandewal, K.; Andrienko, D. Open-circuit voltage of organic solar cells: interfacial roughness makes the difference. *Commun. Phys.* **2022**, *5* (1), 307.
(72) Sun, J.; Zhang, Z.; Yin, X.; Zhou, J.; Yang, L.; Geng, R.; Zhang, F.; Zhu, R.; Yu, J.; Tang, W. High performance non-fullerene polymer solar cells based on PTB7-Th as the electron donor with 10.42% efficiency. *J. Mater. Chem. A* **2018**, *6* (6), 2549−2554.
(73) Gao, J.; Gao, W.; Ma, X.; Hu, Z.; Xu, C.; Wang, X.; An, Q.; Yang, C.; Zhang, X.; Zhang, F. Over 14.5% efficiency and 71.6% fill factor of ternary organic solar cells with 300 nm thick active layers. *Energy Environ. Sci.* **2020**, *13* (3), 958−967.
(74) Shi, F.; Guo, P.; Qiao, X.; Yao, G.; Zhang, T.; Lu, Q.; Wang, Q.; Wang, X.; Rikhsibaev, J.; Wang, E.; et al. A Nitroxide Radical Conjugated Polymer as an Additive to Reduce Nonradiative Energy Loss in Organic Solar Cells. *Adv. Mater.* **2023**, *35* (23), 2212084.
(75) Chen, J. D.; Cui, C.; Li, Y.; Zhou, L.; Ou, Q.; Li, C.; Li, Y.; Tang, J. Single junction polymer solar cells exceeding 10% power conversion efficiency. *Adv. Mater.* **2015**, *27* (6), 1035−1041.
(76) Yaqoob, U.; Raza Ayub, A.; Rafiq, S.; Khalid, M.; El-Badry, Y. A.; El-Bahy, Z. M.; Iqbal, J. Structural, optical and photovoltaic properties of unfused Non-Fullerene acceptors for efficient solution processable organic solar cell (Estimated PCE greater than 12.4%): A DFT approach. *J. Mol. Liq.* **2021**, *341*, 117428.

https://doi.org/10.1021/acsomega.3c05176
ACS Omega 2023, 8, 42492−42510